

Exploration of Dark Chemical Genomics Space via Portal Learning: Applied to Targeting the Undruggable Genome and COVID-19 Anti-Infective Polypharmacology

Tian Cai¹, Li Xie², Muge Chen³, Yang Liu², Di He¹, Shuo Zhang¹, Cameron Mura⁴, Philip E. Bourne⁴, and Lei Xie^{1,2,5,*}

¹*Ph.D. Program in Computer Science, The Graduate Center, The City University of New York, New York, 10016, USA*

²*Department of Computer Science, Hunter College, The City University of New York, New York, 10065, USA*

³*Master Program in Computer Science, Courant Institute of Mathematical Sciences, New York University*

⁴*School of Data Science & Department of Biomedical Engineering, University of Virginia, Virginia, 22903, USA*

⁵*Helen and Robert Appel Alzheimer's Disease Research Institute, Feil Family Brain & Mind Research Institute, Weill Cornell Medicine, Cornell University, New York, 10021, USA*

**lei.xie@hunter.cuny.edu*

November 30, 2021

Abstract

Advances in biomedicine are largely fueled by exploring uncharted territories of human biology. Machine learning can both enable and accelerate discovery, but faces a fundamental hurdle when applied to unseen data with distributions that differ from previously observed ones—a common dilemma in scientific inquiry. We have developed a new deep learning framework, called *Portal Learning*, to explore dark chemical and biological space. Three key, novel components of our approach include: (i) end-to-end, step-wise transfer learning, in recognition of biology's sequence-structure-function paradigm, (ii) out-of-cluster meta-learning, and (iii) stress model selection. Portal Learning provides a practical solution to the out-of-distribution (OOD) problem in statistical machine learning. Here, we have implemented Portal Learning to predict chemical-protein interactions on a genome-wide scale. Systematic studies demonstrate that Portal Learning can effectively assign ligands to unexplored gene families (unknown functions), versus existing state-of-the-art methods, thereby allowing us to target previously “undruggable” proteins and design novel polypharmacological agents for disrupting interactions between SARS-CoV-2 and human proteins. Portal Learning is general-purpose and can be further applied to other areas of scientific inquiry.

1 Introduction

The central aim of scientific inquiry has been to deduce new concepts from existing knowledge or generalized observations. The biological sciences offer numerous such challenges. The rise of deep learning has spurred major interest in using machine learning to explore uncharted molecular and functional spaces in biology and medicine, ranging from ‘deorphanizing’ G-protein coupled receptors[1] and translating cell-line screens to patient drug responses[2][3], to predicting novel protein structures[4][5][6], to identifying new cell types from single-cell omics data[7]. Illuminating the dark space of human knowledge is a fundamental problem that one can attempt to address via deep learning—that is, to generalize a “well-trained” model to unseen data that lies out-of-the-distribution (OOD) of the training data, in order to successfully predict outcomes from conditions that the model has never before encountered. While deep learning is capable, in theory, of simulating any functional mapping, its generalization power is notoriously limited in the case of distribution shifts[8].

The training of a deep learning model starts with a domain-specific model architecture. The final model instance that is selected, and its performance, are determined by a series of data-dependent design choices, including model initialization, data used for training, validation, and testing, optimization of loss function, and evaluation metrics. Each of these design choices impacts the generalization power of a trained model. The development of several recent deep learning-based approaches—notably transfer learning[9], self-supervised representation learning[10], and meta-learning [11][12]—has been motivated by the OOD challenge. However, each of these methods focuses on only one aspect in the training pipeline of a deep model. Causal learning and mechanism-based modeling could be a more effective solution to the OOD problem [8], but at present these approaches can be applied only on modest scales because of data scarcity and limited domain knowledge. Solving large-scale OOD problems in biomedicine, via machine learning, would benefit from a systematic framework for integrative, beginning-to-end model development, training, and testing.

Here, we propose a new deep learning framework, called *Portal Learning*, that systematically addresses the three OOD vulnerabilities in a training pipeline: specifically, we employ biology-inspired model initialization, optimization on an OOD loss, and model selection methods. We define ‘*portal*’ as a model with an initialized instance that is (preferably) close to the global optimum in some learning ‘*universe*’. The *universe* includes a specific input data-set, specific tasks, and a model architecture that provides a functional mapping from the data-set (and associated distributions) to the tasks. Note that, even with the same model architecture, changes in a pipeline’s associated data-set correspond to changes in the universe. Portal Learning takes a global view to design training schemes that are task-specific and use domain knowledge as constraints to guide the exploration of the learning space.

To assess the utility of Portal Learning, we implemented this concept as a concrete framework, termed *PortalCG*, for predicting small-molecule binding to dark gene families (i.e., those with no annotated ligands). Despite tremendous progress in high-throughput screening, the majority of chemical genomics space remains unexplored or ‘dark’ [13] (more details in results). Elucidating dark gene families can illuminate many fundamental but only poorly characterized biological pathways, such as microbiome-host interactions mediated by metabolite-protein interactions. Such efforts could also provide novel approaches for identifying new druggable targets and discovering effective therapeutic strategies for currently incurable diseases; for instance, in Alzheimer’s disease (AD) many disease-associated genes have been identified from multiple omics studies, but are currently considered un-druggable [14]. Accurately predicting chemical-protein interactions (CPIs) on a genome-wide scale is a challenging OOD problem[1]. If one considers only the reported area under the receiver operating characteristic curve (AUROC), which has achieved 0.9 in many state-of-the-art methods[15][16], it may seem the problem has been solved. However, the performance has been primarily measured in scenarios where the data distribution in the test set does not differ significantly from that in the training set, in terms of identities of proteins or types of chemicals. Few sequence-based methods have been developed and evaluated for an out-of-gene family scenario, where proteins in the test set belong to different (non-homologous) gene families than in the training set; this sampling bias is even more severe in considering cases where the new gene family does not have any reliable three-dimensional (3D) structural information. Therefore, one can fairly claim that all existing work has been confined to just narrow regions of chemical genomics space, without validated generalizability into the dark genome.

Rigorous benchmarking studies, reported herein, show that PortalCG significantly outperforms the leading methods that are available for predicting ligand binding to (dark) proteins. We applied PortalCG to predict candidate drug compounds for undrugged disease genes in the dark human genome, and we prioritized hundreds of undrugged genes that can be efficaciously targeted by existing drugs (notably, many of which involve alternative splicing and transcription factor). These novel genes and their lead compounds provide new opportunities for drug discovery. Furthermore, using PortalCG, we identified polypharmacological agents that might leverage novel drug targets in order

to disrupt interactions between SARS-CoV-2 and human proteins. The rapid emergence of SARS-CoV-2 variants has posed a significant challenge to existing vaccine and anti-viral development paradigms. Gordon et al. experimentally identified 332 human proteins that interact with the SARS-CoV-2 virus[17]. This PPI map provides unique opportunities for anti-SARS-CoV-2 drug discovery: targeting the host proteins involved in PPIs can disrupt human SARS-CoV-2 interactions, thereby thwarting the onset of COVID-19. By not aiming to directly kill virions, this indirect strategy should lessen the selection pressure on viral genome evolution. A polypharmacological agent that interacts moderately strongly with multiple human proteins could be a potentially quite effective and safe anti-COVID-19 therapeutic: on the one hand, the normal functions of human proteins should not be significantly perturbed while, on the other hand, the interactions required for successful SARS-CoV-2 infection would be inhibited. Here, we virtually screened compounds in the Drug Repurposing Hub[18] against the 332 human SARS-CoV-2 interactors. Two drugs, Fenebrutinib and NMS-P715, ranked highly; interestingly, both of these anti-tumorigenic compounds inhibit kinases. Their interactions with putative human targets were supported by further (structure-based) analyses of protein-ligand binding poses.

In summary, the contributions of this work are three-fold:

1. A novel, generalized training scheme, *Portal Learning*, is proposed as a way to guide biology-inspired systematic design in order to improve the generalization power of machine learning on OOD problems, such as is found in the dark regions of molecular/functional space.
2. To concretely illustrate the Portal Learning approach, a specific algorithm, PortalCG, is proposed and implemented. Comprehensive benchmark studies demonstrate the promise of PortalCG when applied to OOD problems, specifically for exploring the dark regions of chemical genomics space.
3. Using PortalCG, we shed new light on unknown protein functions in dark genomes (viz. small molecule-binding properties), and open new avenues in polypharmacology and drug repurposing; as demonstrated by identifying novel drug targets and lead compounds for AD and anti-SARS-CoV-2 polypharmacology.

2 Conceptual basis of Portal Learning

data split	Common practice	classic scheme applied in OOD	Portal learning	specification
train	IID train	IID train	/	each batch is from the same distribution
	/	/	OOD train	differentiate sub-distributions in each batch
dev	IID-dev	IID-dev	/	from the same distribution as the train set
	/	/	OOD-dev	from a different distribution from the training set
test	IID-test	/	/	from the same distribution as the training set
	/	OOD-test	OOD-test	from a different distribution from both OOD-dev and training set

Table 1: Data split for stress model instance selection

To enable the exploration of dark regions of chemical and biological space, Portal Learning rests upon a systematic, well-principled training strategy, the underpinnings of which are shown in Figure 1. In Portal Learning, a model architecture together with a data set and a task defines a **universe**. Each universe has some global optimum with respect to the task based on a pre-defined loss function. The model-initialized instance in a universe—which could be a local optimum in the current universe, but which facilitates moving the model to the global optimum in the ultimately targeted universe—is called a **portal**. The portal is similar to a catalyst that lowers the energy barrier via a transition state for a chemical reaction to occur. The dark chemical genomics space cannot be explored effectively if the learning process is confined only to the observed universe of protein sequences that have known ligands, as the known data are highly sparse and biased (details in Result section). Hence, it is critical to successfully identify portals into the dark chemical genomics universe starting from the observed protein sequence and structure universe. For clarity and ease of reference, key terms related to Portal Learning are given in the Supplemental Materials.

The remainder of this section describes the three key components of the Portal Learning approach—namely, end-to-end step-wise transfer learning (STL), out-of-cluster meta-learning (OOC-ML), and stress model selection.

End-to-end step-wise transfer learning (STL). Information flow in biological systems generally involves multiple intermediate steps, from a source instance to a target. For example, a discrete genotype (source) ultimately yields a downstream phenotype (target) via many steps of gene expression, in some environmental context. For predicting genotype-phenotype associations, explicit machine learning models that represent information transmission from DNA to RNA to cellular phenotype are more powerful than those that ignore the intermediate steps [19]. In Portal

Learning, transcriptomics profiles can be used as a portal to link the source genetic variation (e.g., variants, SNPs, homologs, etc.) and target cellular phenotype (e.g., drug sensitivity). Using deep neural networks, this process can be modeled in an end-to-end fashion.

Out-of-cluster meta-learning (OOC-ML). Even if we can successfully transfer the information needed for the target through intermediate portals from the source universe, we still need additional portals to reach those many sparsely-populated regions of the dark universe that lack labeled data in the target. Inspired by Model Agnostic Meta-Learning (MAML)[11], we designed a new OOC-ML approach to explore the dark biological space. MAML cannot be directly applied to Portal Learning in the context of the OOD problem because it is designed for few-shot learning under a multi-task formulation. Few-shot learning expects to have a few labeled samples from the test data set to update the trained model during inference for a new task. This approach cannot be directly applied to predicting gene functions of dark gene families where the task (e.g., binary classification of ligand binding) is unchanged, but rather there are no labeled data for a unseen distribution that may differ significantly from the training data. In a sense, rather than MAML’s "few-shot/multi-task" problem context, mapping dark chemical/biological space is more of a "zero-shot/single-task" learning problem. A key insight of OOC-ML is to define sub-distributions (clusters) for the labeled data in the source instance universe. An example demonstrated in this paper is to define sub-distributions using Pfam families when the source instance is a protein sequence. Intuitively, OOC-ML involves a two-stage learning process. In the first stage, a model is trained using each individual labeled cluster (e.g., a given Pfam ID), thereby learning whatever knowledge is (implicitly) specific to each cluster. In the second stage, all trained models from the first stage are combined and a new ensemble model is trained, using labeled clusters that were not used in the first stage. In this way, we may extract common intrinsic patterns shared by all clusters and apply the learned essential knowledge to dark ones.

Stress model selection. Finally, training should be stopped at a suitable point in order to avoid overfitting. This was achieved by stress model selection. Stress model selection is designed to basically recapitulate an OOD scenario by splitting the data into OOD train, OOD development, and OOD test sets as listed in Table 1; in this procedure, the data distribution for the development set differs from that of the training data, and the distribution of the test data set differs from both the training and development data.

For additional details and perspective, the conceptual and theoretical basis of Portal Learning is further described in the Methods section of the Supplemental Materials.

3 Results and Discussion

3.1 Overview of PortalCG

We implemented the Portal Learning concept as a concrete model, PortalCG, for exploring the dark chemical genomics space. In terms of Portal Learning’s three key components (STL, OOC-ML, and stress model selection), PortalCG makes the following design choices (see also Figure 2).

End-to-end sequence-structure-function STL. The function of a protein—e.g., serving as a target receptor for ligand binding—stems from its three-dimensional (3D) shape and dynamics which, in turn, is ultimately encoded in its primary amino acid sequence. In general, information about a protein’s structure is more powerful than purely sequence-based information for predicting its molecular function because sequences drift/diverge far more rapidly than do 3D structures on evolutionary timescales. Although the number of experimentally-determined structures continues to exponentially increase, and now AlphaFold2 can reliably predict 3D structures of most single-domain proteins, it nevertheless remains quite challenging to directly use protein structures as input for predicting ligand-binding properties of dark proteins. In PortalCG, protein structure information is used as a portal to connect a source protein sequence and a corresponding target protein function (Figure 1A). We begin by performing self-supervised training to map tens of millions of sequences into a universal embedding space, using our recent *distilled sequence alignment embedding* (DISAE) algorithm [1]. Then, 3D structural information about the ligand-binding site is used to fine-tune the sequence embedding. Finally, this structure-regularized protein embedding was used as a hidden layer for supervised learning of cross-gene family CPIs, following an end-to-end sequence-structure-function training process. By encapsulating the role of structure in this way, inaccuracies and uncertainties in structure prediction are ‘insulated’ and will not propagate to the function prediction.

Out-of-cluster meta-learning. In the OOC-ML framework, Pfam gene families provide natural clusters as sub-distributions. In each Pfam family, the data is split into support set and query set as shown in Figure 1(B). Specifically, a model is trained for a single Pfam family independently to reach a local minimum using the support set of the Pfam family as shown in the inner loop IID optimization in Figure 1(C.1). Then a query set from the same Pfam family is used on the locally optimized model to get a loss from the local loss landscape, i.e. outer loop IID meta optimization

in Figure 1(C.1). Local losses from the query sets of multiple Pfam families will be aggregated to calculate the loss on a global loss landscape, i.e. meta optimization in Figure 1(C.1). For some cluster with very limited number of data, they don't have a support set hence will only participate in the optimization on the global loss landscape. There could be many choices of aggregations. A simple way is to calculate the average loss. The aggregated loss will be used to optimize the model on the global loss landscape. Note that weights learned on each local loss landscape will be memorized during the global optimization. In our implementation, it is realized by creating a copy of the model trained from the each family's local optimization. In this way, the local knowledge learned is ensured to be only passed to the global loss landscape by the query set loss.

Stress model selection. The final model was selected using Pfam families that were not used in the training stage (Figure 2, right panel).

The Supplemental Materials provide further methodological details, covering data pre-processing, the core algorithm, model configuration, and implementation details.

3.2 There are significantly unexplored dark spaces in chemical genomics

We inspected the known CPIs between (i) molecules in the manually-curated ChEMBL database, which consists of only a small portion of all chemical space, and (ii) proteins annotated in Pfam-A [20], which represents only a narrow slice of the whole protein sequence universe. The ChEMBL26[21] database supplies 1,950,765 chemicals paired to 13,377 protein targets, constituting 15,996,368 known interaction pairs. Even for just this small portion of chemical genomics space, unexplored CPIs are enormous, can be seen in the dark region in Figure 3. Approximately 90% of Pfam-A families do not have any known small-molecule binder. Even in Pfam families with annotated CPIs (e.g., GPCRs), there exists a significant number of 'orphan' receptors with unknown cognate ligands (Figure 3). Fewer than 1% of chemicals bind to more than two proteins, and < 0.4% of chemicals bind to more than five proteins, as shown in Supplemental Figures S1, S2 and S3. Because protein sequences and chemical structures in the dark chemical genomics space could be significantly different from those for the known CPIs, predicting CPIs in the dark space is an archetypal, unaddressed OOD problem.

3.3 Portal Learning significantly outperforms state-of-the-art approaches to predicting dark CPIs

When compared with the state-of-the-art method DISAE[1], which already was shown to outperform other leading methods for predicting CPIs of orphan receptors, PortalCG demonstrates superior performance in terms of both Receiver Operating Characteristic (ROC) and Precision-Recall (PR) curves, as shown in Figure 4(a). Because the ratio of positive and negative cases is imbalanced, the PR curve is more informative than the ROC curve. The PR-AUC of PortalCG and DISAE is 0.714 and 0.603, respectively. In this regard, the performance gain of Portal Learning (18.4%) is significant (p-value < $1e - 40$). Performance breakdowns for binding and non-binding classes can be found in Supplemental Figure S4.

PortalCG exhibits much higher recall and precision scores for positive cases (i.e., a chemical-protein pair that is predicted to bind) versus negative, as shown in Supplemental Figure S4; this is a highly encouraging result, given that there are many more negative (non-binding) than positive cases. The deployment gap, shown in Figure 4(b), is steadily around zero for PortalCG; this promising finding means that we can expect that, when applied to the dark genomics space, the performance will be similar to that measured using the development data set.

With the advent of high-accuracy protein structural models, predicted by AlphaFold2 [5], it now becomes feasible to use reversed protein-ligand docking (RPLD)[22] to predict ligand-binding sites and poses on dark proteins, on a genome-wide scale. In order to compare our method with the RPLD approach, blind docking to putative targets was performed via Autodock Vina[23]. After removing proteins that failed in the RPLD experiments (mainly due to extended structural loops), docking scores for 28,909 chemical-protein pairs were obtained. The performance of RPLD was compared with that of PortalGC and DISAE. As shown in Figure 4(a), both ROC and PR for RPLD are significantly worse than for PortalGC and DISAE. It is well known that PLD suffers from a high false-positive rate due to poor modeling of protein dynamics, solvation effects, crystallized waters, and other challenges [24]; often, small-molecule ligands will indiscriminately 'stick' to concave, pocket-like patches on protein surfaces. For these reasons, although AlphaFold2 can accurately predict many protein structures, the relatively low reliability of PLD still poses a significant limitation, even with a limitless supply of predicted structures [25]. Thus, the direct application of RPLD remains a challenge for predicting ligand binding to dark proteins. PortalCG's end-to-end sequence-structure-function learning could be a more effective strategy: protein structure information is not used as a fixed input, but rather as an intermediate layer that can be tuned using various structural and

functional information. From this perspective, again the role of protein structure in PortalCG can be seen as that of a portal (sequence→function; Figure 1) and a regularizer (Figure 2).

3.4 Both the STL and OOC-ML stages contribute to the improved performance of PortalCG

	models	PR-AUC (OOD-test set)	ROC-AUC (OOD-test set)	ROC-AUC Deployment Gap	PR-AUC Deployment Gap
DIASE	PortalCG w/o STL & OOC-ML	0.603±0.005	0.636±0.004	-0.275±0.016	-0.345±0.012
variant 1	PortalCG w/o OOC-ML	0.629±0.005	0.661±0.004	—	—
variant 2	PortalCG w/o STL	0.698±0.015	0.654±0.062	—	—
PortalCG	Portal learning	0.714±0.010	0.677±0.010	0.010±0.009	0.005±0.010

Table 2: Ablation study of PortalCG.

To gauge the potential contribution of each component of PortalCG to the overall system effectiveness in predicting dark CPIs, we systematically compared the four models shown in Table 2. Details of the exact model configurations for these experiments can be found in the Supplemental Materials Table S10 and Figure S13. As shown in Table 2, Variant 1, with a higher PR-AUC compared to the DISAE baseline, is the direct gain from transfer learning through 3D binding site information, all else being equal; yet, with transfer learning alone and without OOC-ML as an optimization algorithm in the target universe (i.e., Variant 2 versus Variant 1), the PR-AUC gain is minor. Variant 2 yields a 15% improvement while Variant 1 achieves only a 4% improvement. PortalCG (i.e., full Portal Learning), in comparison, has the best PR-AUC score. With all other factors held constant, the advantage of PortalCG appears to be the synergistic effect of both STL and OOC-ML. The performance gain measured by PR-AUC under a shifted evaluation setting is significant (p-value < 1e-40), as shown in Supplemental Figure S5.

We find that stress model selection is able to mitigate potential overfitting problems, as expected. Training curves for the stress model selection are in Supplemental Figures S4 and S6. As shown in Supplemental Figure S6, the baseline DISAE approach tends to over-fit with training, and IID-dev performances are all higher than PortalCG but deteriorate in OOD-test performance. Hence, the deployment gap for the baseline is -0.275 and -0.345 on ROC-AUC and PR-AUC, respectively, while PortalCG deployment is around 0.01 and 0.005, respectively.

3.5 Application of PortalCG to explore dark chemical genomics space

A production-level model using PortalCG was trained with ensemble methods for the deployment. Details are in the Supplemental Methods section. The trained PortalCG model was applied to two case-studies in order to assess its utility in the exploration of dark space. As long as a protein and chemical pair was presented to this model with their respective sequence and SMILES string, a prediction could be made, along with a corresponding prediction score. To select high confidence predictions, a histogram of prediction scores was built based on known pairs (Supplemental Figure S7). A threshold of 0.67, corresponding to a false positive rate of 2.18e-05, was identified to filter out high-confidence positive predictions. Around 6,000 drugs from the Drug Repurposing Hub[26] were used in the screening. The remainder of this section describes the two case-studies that were examined with PortalCG, namely (i) COVID-19 polypharmacology and (ii) the ‘undruggable’ portion of the human genome.

3.5.1 COVID-19 polypharmacology

In order to identify lead compounds that may disrupt SARS-CoV-2-Human interactions, we screened 5,886 approved and investigational drugs against the 332 human proteins known to interact with SARS-CoV-2. We considered a drug-protein pair as a positive hit and selected it for further analysis only when all models in an ensemble vote as positive and the false positive rate does not exceed 2.18e-05. Drugs involved in these positive pairs were ranked according to the number of proteins to which they are predicted to bind. Detailed information is given in Supplemental Table S1. Most of these drugs are protein kinase inhibitors and are already in Phase 2 clinical trials. Among them, Fenebrutinib and NMS-P715 are predicted to bind to seven human SARS-CoV-2 interactors, as shown in Table 3. In order to elucidate how these drug molecules might associate with a SARS-CoV-2 interactor partner, we performed molecular docking for Fenebrutinib and NMS-P715. Structures of two SARS-CoV-2 interactors were obtained from the Protein Data Bank; the remaining five proteins do not have experimentally solved structures so their predicted structures (via AlphaFold2) were used for docking. For most of these structures, the binding pockets are unknown. Therefore, blind docking was employed, using Autodock Vina[23] to search the full surfaces (the accessible molecular envelope) and identify putative binding sites of Fenebrutinib and NMS-P715 on these

interactors. Docking conformations with the best (lowest) predicted binding energies were selected for each protein; the respective binding energies are listed in Table 3.

Components of the exosome complex are predicted targets for both Fenebrutinib and NMS-P715. The exosome complex is a multi-protein, intracellular complex which is involved in degradation of many types of RNA molecules (e.g., via 3'→5' exonuclease activities). As shown in Figure 5, the subunits of the exosomal assembly form a central channel; RNA passes through this region as part of the degradation/processing. Intriguingly, SARS-CoV-2's genomic RNA has been found to be localized in the exosomal cargo, suggesting a key mechanistic role for the channel region in SARS-CoV-2 virion infectivity pathways [27]. Fenebrutinib and NMS-P715 were also predicted to bind to a specific exonuclease, RRP43, of the exosome complex, while NMS-P715 was also predicted to bind yet another exonuclease, RRP46.

The predicted binding poses for Fenebrutinib and NMS-P715 with the exosomal complex components are shown in Figure 5. The physicochemical/interatomic interactions between these two drugs and the exosome complex components are also schematized as a 2D layout in this figure. The favorable hydrogen bond, pi-alkyl, pi-cation and Van der Waals interactions provide additional support that Fenebrutinib and NMS-P715 do indeed bind to these components of the exosome complex. The predicted binding poses and 2D interactions maps for Fenebrutinib and NMS-P715 with other targeted proteins are shown in Supplementary Figures S8, S9, and S10.

Docking scores of Fenebrutinib binding to predicted targets			
Uniprot ID	Protein name	PDB ID	Docking score (kcal/mol)
Q96B26	Exosome complex component RRP43	2NN6_C	-7.9
Q5JRX3	Presequence protease, mitochondrial	4L3T_A	-10.8
Q99720	Sigma non-opioid intracellular receptor 1	5HK1_A	-9.6
Q5VT66	Mitochondrial amidoxime-reducing component 1	6FW2_A	-10.4
P29122	Proprotein convertase subtilisin/kexin type 6	AF-P29122-F1 (157-622)	-8.5
Q96K12	Fatty acyl-CoA reductase 2	AF-Q96K12-F1 (1-478)	-10.1
O94973	AP-2 complex subunit alpha-2	AF-O94973-F1 (3-622)	-8.6
Docking scores of NMS-P715 binding to predicted targets			
Uniprot ID	Protein name	PDB ID	Docking score (kcal/mol)
Q9UN86	Ras GTPase-activating protein-binding protein 2	5DRV_A	-9.5
P67870	Casein kinase II subunit beta	1QF8_A	-8.6
Q96B26	Exosome complex component RRP43	2NN6_C	-9.3
P62877	E3 ubiquitin-protein ligase RBX1	2HYE_D	-7.9
P61962	DDB1- and CUL4-associated factor 7	AF-P61962-F1 (9-341)	-8.7
Q9NXH9	tRNA (guanine(26)-N(2))-dimethyltransferase	AF-Q9NXH9-F1 (53-556)	-9.0
Q9NQT4	Exosome complex component RRP46	2NN6_D	-8.6

Table 3: Docking scores for Fenebrutinib and NMS-P715

3.5.2 Illuminating the undruggable human genome

It is well known that only a small subset of the human genome is considered druggable [28]. Many proteins are deemed “undruggable” because there is no information on their ligand-binding properties or other interactions with small-molecule compounds (be they endogenous or exogenous ligands). Here, we built an “undruggable” human disease protein database by removing the druggable proteins in Pharos [29] and Casas’s druggable proteins [30] from human disease associated genes [14] and applied PortalCG to predict the probability for these “undruggable” proteins to bind to drug-like molecules. A total of 12,475 proteins were included in our disease-associated undruggable human protein list. These proteins were ranked according to their probability scores, and 267 of them have a false positive rate lower than 2.18e-05, as listed in the supplementary material Table S2. Table 4 shows the statistically significantly enriched functions of these top ranked proteins as determined by DAVID [31]. The most enriched proteins are involved in alternative splicing of mRNA transcripts. Malfunctions in alternative splicing are linked to many diseases, including several cancers [32][33] and Alzheimer’s disease [34]. However, pharmaceutical modulation of alternative splicing process is a challenging task. Identifying new drug targets and their lead compounds for targeting alternative splicing pathways may open new doors to developing novel therapeutics for complex diseases with few treatment options. Diseases associated with these 267 human proteins were also listed in Table 5. Since one protein is always related to multiple diseases, these diseases are ranked by the number of their associated proteins. Most of top ranked diseases are related with cancer development. 21 drugs that are approved or in clinical development are predicted to interact with these proteins as shown in Table S3. Several of these drugs are highly promiscuous. For example, AI-10-49, a molecule that disrupts protein-protein interaction between CBFb-SMMHC and

tumor suppressor RUNX1, may bind to more than 60 other proteins. The off-target binding profile of these proteins may provide invaluable information on potential side effects and opportunities for drug repurposing and polypharmacology. The drug-target interaction network built for predicted positive proteins associated with Alzheimer’s disease was shown in Figure 6. Functional enrichment, disease associations, and top ranked drugs for the undruggable proteins with well-studied biology (classified as Tbio in Pharos) and those excluding Tbio are list in Supplemental Table S4-S9.

David Functional Annotation enrichment analysis				
Enriched terms in UniProtKB keywords	Number of proteins involved	Percentage of proteins involved	P-value	Modified Benjamini p-value
Alternative splicing	171	66.5	7.70E-07	2.00E-04
Phosphoprotein	140	54.5	2.60E-06	3.40E-04
Cytoplasm	91	35.4	1.30E-05	1.10E-03
Nucleus	93	36.2	1.20E-04	8.10E-03
Metal-binding	68	26.5	4.20E-04	2.20E-02
Zinc	48	18.7	6.60E-04	2.90E-02

Table 4: Functional Annotation enrichment for undruggable human disease proteins selected by PortalCG

DiseaseName	# of undruggable proteins associated with disease
Breast Carcinoma	90
Tumor Cell Invasion	86
Carcinogenesis	83
Neoplasm Metastasis	75
Colorectal Carcinoma	73
Liver carcinoma	66
Malignant neoplasm of lung	56
Non-Small Cell Lung Carcinoma	56
Carcinoma of lung	54
Alzheimer’s Disease	54

Table 5: Top ranked diseases associated with the undruggable human disease proteins selected by PortalCG

4 Conclusion

This paper confronts the challenge of exploring dark chemical genomics space by recognizing it as an OOD generalization problem in machine learning, and by developing a new learning framework to treat this type of problem. We propose Portal Learning as a general framework that enables systematic control of the OOD generalization risk. As a concrete algorithmic example and use-case, PortalCG was implemented under the Portal Learning framework. Systematic examination of the PortalCG method revealed its superior performance compared to (i) a state-of-the-art deep learning model (DISAE), and (ii) an AlphaFold2-enabled, structure-based reverse docking approach. PortalCG showed significant improvements in terms of both sensitivity and specificity, as well as close to zero deployment performance gap. With this approach, we were able to explore the dark regions of the druggable genome. Applications of PortalCG to COVID-19 polypharmacology and to the targeting of hitherto undruggable human proteins affords novel new directions in drug discovery.

5 Methods

5.1 Full algorithm details

Portal learning as a system level framework involves collaborative new design from data preprocessing, data splitting to model architecture, model initialization, and model optimization and evaluation. The main illustrations are Figure 1 and Figure 2. Extensive explanation of each of the component and their motivations are available in Supplemental Materials section Methods with Figure S11, and Algorithm1.

5.2 Data

PortalCG uses three database, Pfam[20], Protein Data Bank (PDB)[35] and ChEMBL[21]. Two applications are demonstrated, COVID-19 polypharmacology and undruggable human proteins, for which known approved drugs are collected from CLUE[26], 332 human proteins interacting SARS-CoV-2 are listed in recent publication[36], 12,475 undruggable proteins are collected by removing the druggable proteins in Pharos [29] and Casas’s druggable proteins [30] from human disease associated genes [14]. Detailed explanation of how each data set is used can be found in Supplemental Materials Methods section.

Major data statistics are demonstrated in Figure 3 and Supplemental Materials Figure S1, S2, and S3.

5.3 Experiment implementation

Experiments are first organized to test PortalCG performance against baseline models, DISAE[1] and AlphaFold2[5]. DISAE is a protein language which predicts protein function based on protein sequence information alone. AlphaFold2 uses protein sequence information to predict protein structure, combining docking methods, can be used to predict protein function. Main results are shown with Table 2 and Figure 4. Ablation studies is also performed mainly to test some variants of PortalCG components such as binding site distance prediction as shown in Supplemental Figure S12. Since Portal Learning is a general framework, there could be many interesting variants to pursue in future studies. To enhance application accuracy, a production level model is built with ensemble learning, and high confidence predictions are selected as demonstrated in Supplemental Material Figure S7. Evaluation metrics used are F1, ROC-AUC and PR-AUC.

Extensive details can be found in Supplemental Materials Methods section.

5.4 Related works

A literature review of related works could be found in Supplemental Materials section Related Works.

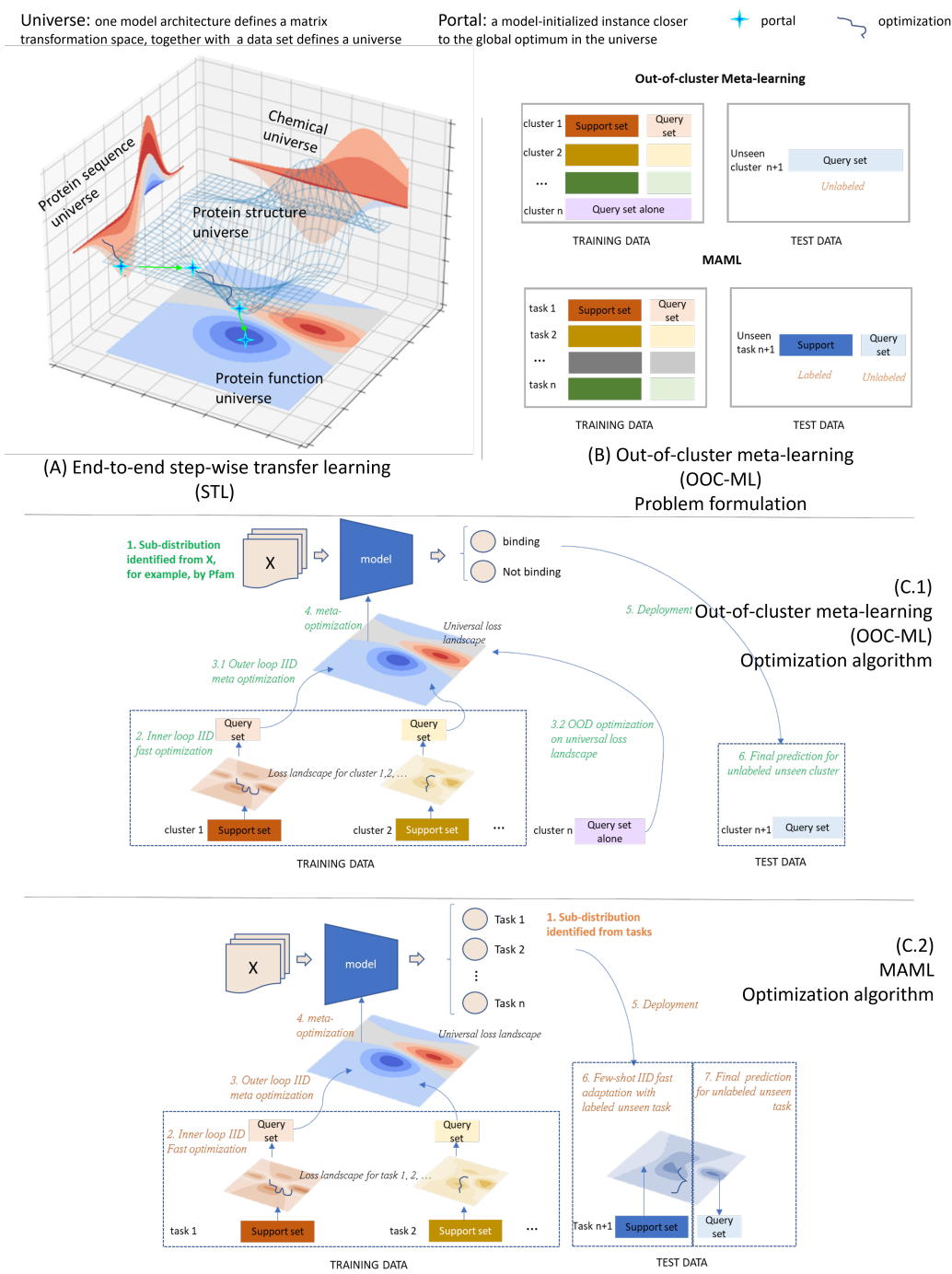


Figure 1: Illustration of two of the three major Portal Learning components for OOD problems, End-to-end step-wise transfer learning (STL) and out-of-cluster meta-learning (OOC-ML), using the prediction of out-of-gene family chemical-protein interactions (CPIs) as an example: **A. STL:** 3D structure of protein ligand binding site is in the center connecting protein sequences to CPIs. There are two portals, the first traveling from the protein sequence universe to the binding site structure universe by pre-training a protein language model that is optimal in the protein sequence universe and leads to a model initialization instance closer to the global optimum in the binding site structure universe. The optimization based on this initialized instance leads to the discovery of the second portal through which protein function universe gets a model initialization instance closer to its own global optimum. **B. Problem formulation of OOC-ML in comparison with MAML:** Different from MAML where training data is grouped based on the task, the training data in OOC-ML is clustered in the instance space. Instead of decomposing the data in all clusters into support and query set like MAML, there is only a query set in certain training clusters and all testing clusters in OOC-ML to simulate OOD scenario. **C. Optimization of OOC-ML in comparison with MAML:** Intuitively, OOC-ML first performs local optimizations on each cluster of training data with the support/query decomposition, then meta optimizations on the training set that has only query sets by ensembling the knowledge learned from the local optimization. The optimized model is applied to the test data in a zero-shot learning setting. In contrast, the meta-optimization in MAML requires query sets in the setting of few-shot learning.

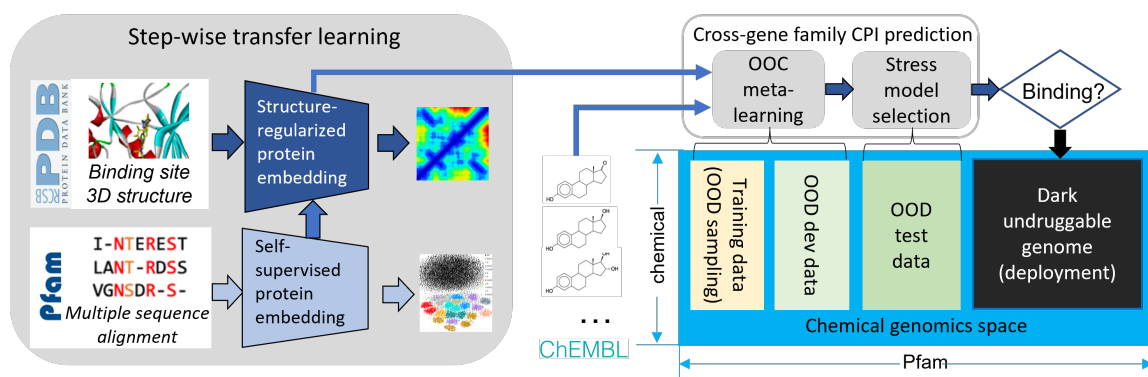


Figure 2: Scheme of PortalCG. PortalCG enables to predict chemical protein interactions (CPIs) for dark genes across gene families. It includes three key components: end-to-end transfer learning following sequence-structure-function paradigm, Out-of-cluster (OOO) meta-learning, and stress model selection.

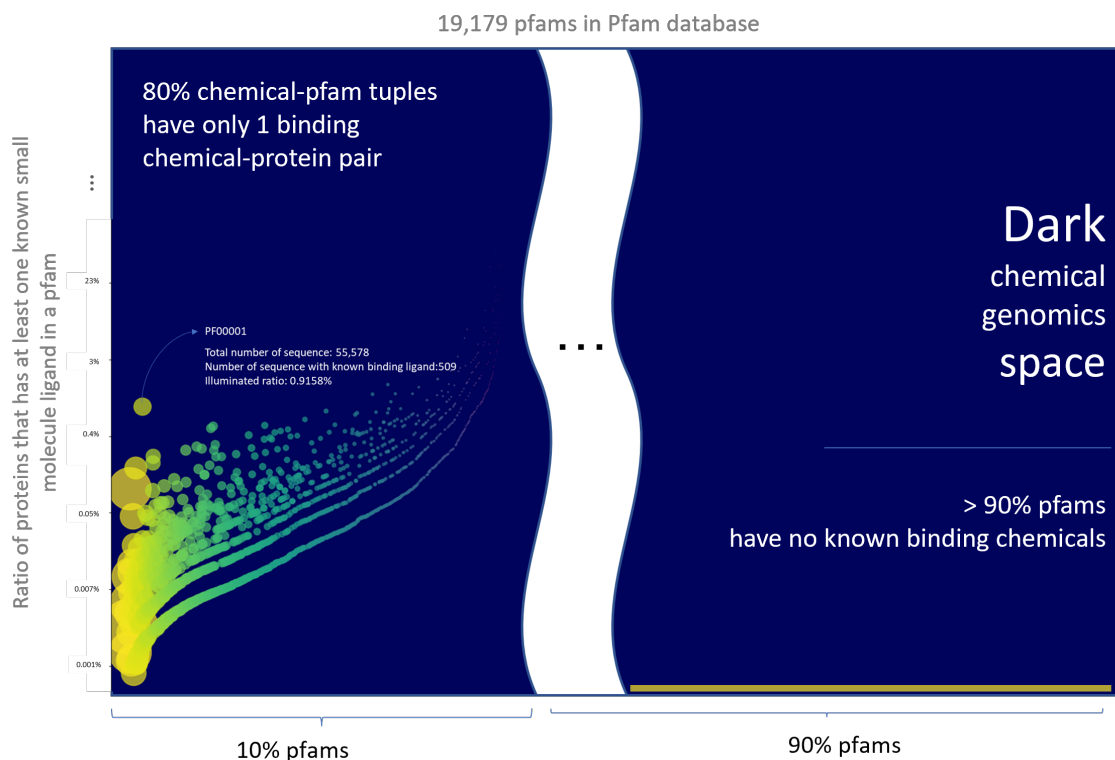


Figure 3: **Chemical genomics space in statistics: The ratio of proteins that have at least a known ligand in each Pfam family.** Each color bubble represents a Pfam family. The size of a bubble is proportional to the total number of proteins in the Pfam family. Y-axis is the ratio of proteins with known ligand(s) in a Pfam family. Around 2,000 Pfam families have at least one known small molecule ligand. Most of these Pfam families have less than 1% proteins with known ligands. Furthermore, around 90% of total 19,179 Pfam families are in the dark chemical genomics space without any known ligand information.

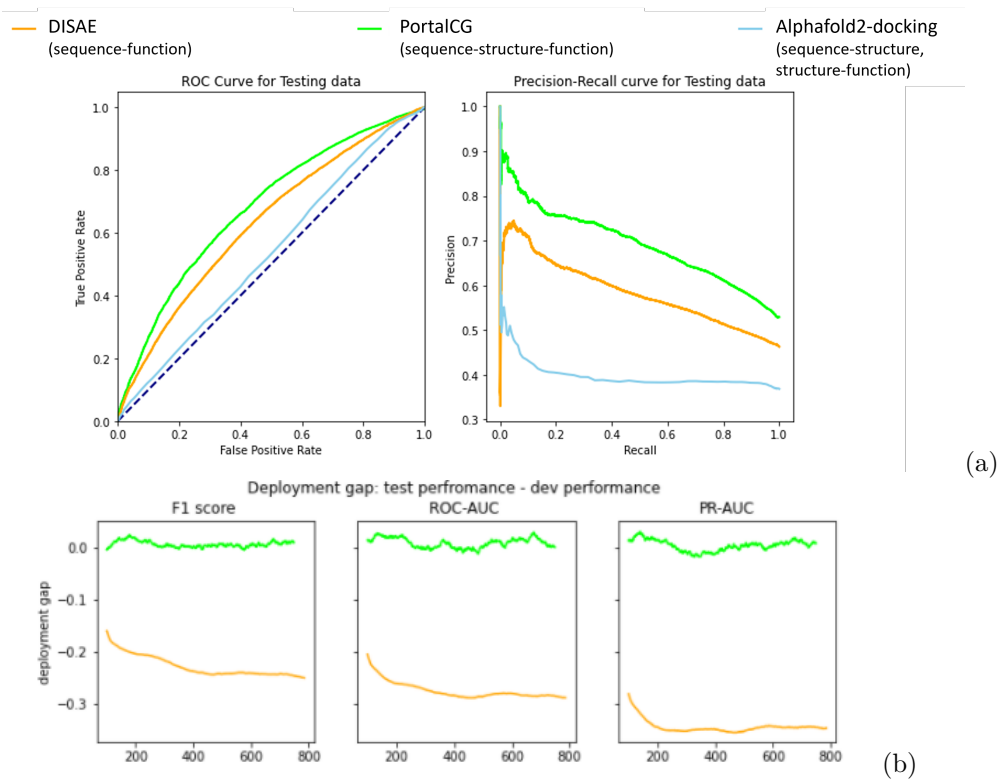


Figure 4: Comparison of PortalCG with the state-of-the-art method DISAE as baseline using the shifted evaluation test. (a) ROC and Precision-Recall curves for the “best” model instance selected by stress test; (b) Deployment gaps where the deployment gap of PortalCG is steadily around zero as training step increases while the deployment performance of DISAE deteriorates.

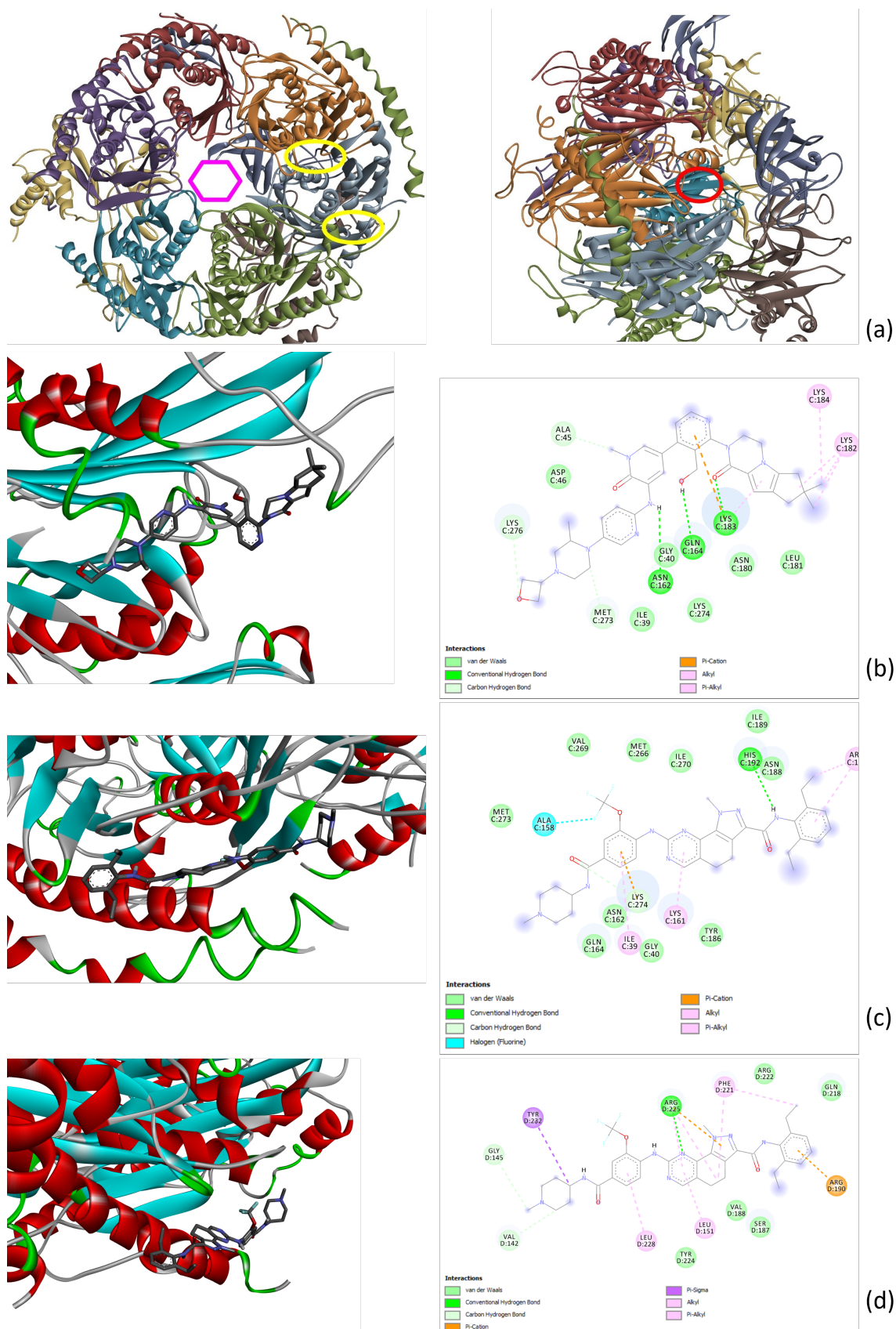


Figure 5: The 3D structure of the exosome complex and the binding conformations of Fenebrutinib and NMS-P715 on the complex components predicted by using Autodock: (a) The exosome complex structure; Left: yellow circles shows the binding pocket of NMS-P715 on RRP43 and RRP46, purple hexagon shows the gate; Right: red circle shows the binding pocket of Fenebrutinib on RRP43. (b) Fenebrutinib on RRP43. (c) NMS-P715 on RRP43. (d) NMS-P715 on RRP46.

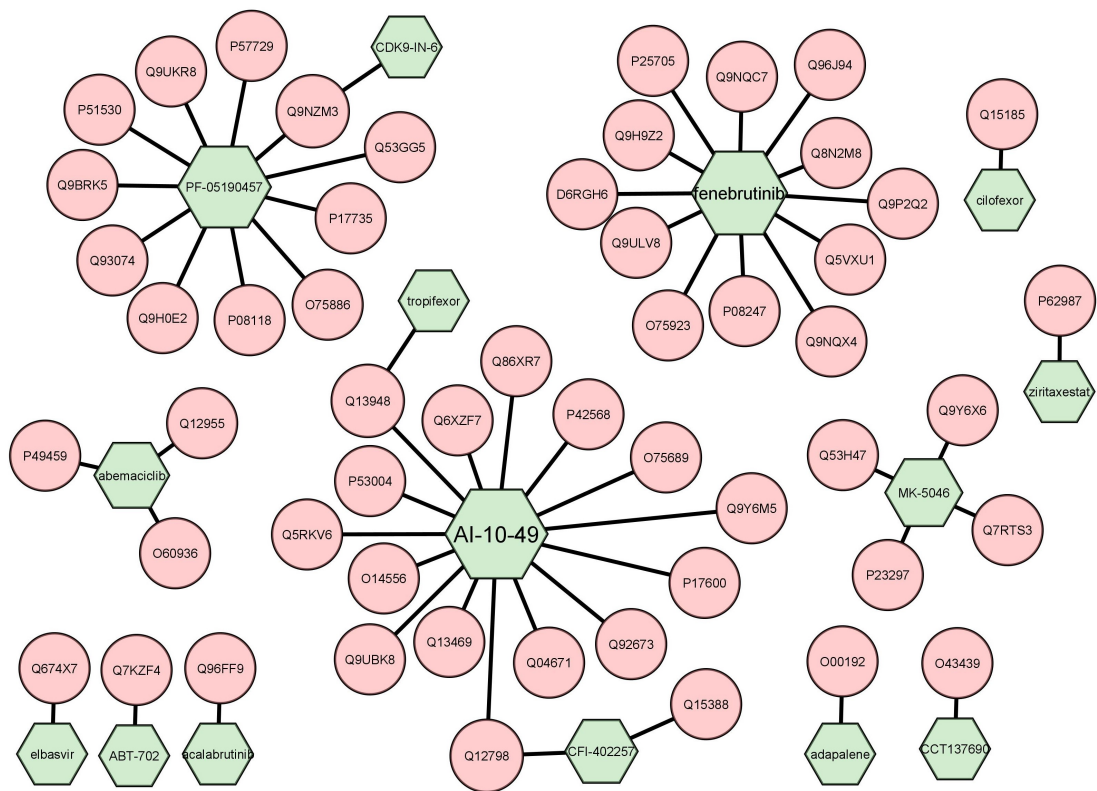


Figure 6: Drug-target interaction network for proteins associated with Alzheimer's disease. Green represents drugs and pink represents targets.

Author Contributions

TC conceived the concept of Portal Learning, implemented the algorithms, performed the experiments, and wrote the manuscript; Li Xie prepared data, performed the experiments, and wrote the manuscript; MC implemented algorithms; YL implemented algorithms; SZ prepared data; CM and PEB refined the concepts and wrote the manuscript; Lei Xie conceived and planned the experiments, wrote the manuscript.

Data and software availability

Data, a pre-trained PortalCG model, and PortalCG codes can be found in the following link: <https://github.com/XieResearchGroup/PortalLearning>

Acknowledgement

This project has been funded with federal funds from the National Institute of General Medical Sciences of National Institute of Health (R01GM122845) and the National Institute on Aging of the National Institute of Health (R01AD057555). We appreciate that Hansaim Lim helped with proof reading and provided constructive suggestions.

References

- [1] T. Cai, H. Lim, K. A. Abbu, Y. Qiu, R. Nussinov, and L. Xie, “Msa-regularized protein sequence transformer toward predicting genome-wide chemical-protein interactions: Application to gprome deorphanization,” *Journal of Chemical Information and Modeling*, vol. 61, no. 4, pp. 1570–1582, 2021.
- [2] J. Ma, S. H. Fong, Y. Luo, C. J. Bakkenist, J. P. Shen, S. Mourragui, L. F. Wessels, M. Hafner, R. Sharan, J. Peng, *et al.*, “Few-shot learning creates predictive models of drug response that translate from high-throughput screens to individual patients,” *Nature Cancer*, vol. 2, no. 2, pp. 233–244, 2021.
- [3] D. He, Q. Liu, and L. Xie, “Robust prediction of patient-specific clinical response to unseen drugs from in vitro screens using context-aware deconfounding autoencoder,” *bioRxiv*, 2021.
- [4] N. Hiranuma, H. Park, M. Baek, I. Anishchenko, J. Dauparas, and D. Baker, “Improved protein structure refinement guided by deep learning based accuracy estimation,” *Nature communications*, vol. 12, no. 1, pp. 1–11, 2021.
- [5] J. Jumper, R. Evans, A. Pritzel, T. Green, M. Figurnov, O. Ronneberger, K. Tunyasuvunakool, R. Bates, A. Žídek, A. Potapenko, *et al.*, “Highly accurate protein structure prediction with alphafold,” *Nature*, pp. 1–11, 2021.
- [6] M. Baek, F. DiMaio, I. Anishchenko, J. Dauparas, S. Ovchinnikov, G. R. Lee, J. Wang, Q. Cong, L. N. Kinch, R. D. Schaeffer, *et al.*, “Accurate prediction of protein structures and interactions using a 3-track network,” *bioRxiv*, 2021.
- [7] Y. Li, P. Luo, Y. Lu, and F.-X. Wu, “Identifying cell types from single-cell data based on similarities and dissimilarities between cells,” *BMC bioinformatics*, vol. 22, no. 3, pp. 1–18, 2021.
- [8] B. Schölkopf, F. Locatello, S. Bauer, N. R. Ke, N. Kalchbrenner, A. Goyal, and Y. Bengio, “Toward causal representation learning,” *Proceedings of the IEEE*, vol. 109, no. 5, pp. 612–634, 2021.
- [9] W. Chen, Z. Yu, Z. Wang, and A. Anandkumar, “Automated synthetic-to-real generalization,” in *International Conference on Machine Learning*, pp. 1746–1756, PMLR, 2020.
- [10] Z. Lan, M. Chen, S. Goodman, K. Gimpel, P. Sharma, and R. Soricut, “Albert: A lite bert for self-supervised learning of language representations,” *arXiv preprint arXiv:1909.11942*, 2019.
- [11] C. Finn, P. Abbeel, and S. Levine, “Model-agnostic meta-learning for fast adaptation of deep networks,” *CoRR*, vol. abs/1703.03400, 2017.
- [12] T. M. Hospedales, A. Antoniou, P. Micaelli, and A. J. Storkey, “Meta-learning in neural networks: A survey,” *CoRR*, vol. abs/2004.05439, 2020.
- [13] T. I. Oprea, “Exploring the dark genome: implications for precision medicine,” *Mammalian Genome*, vol. 30, no. 7, pp. 192–200, 2019.
- [14] J. Piñero, J. M. Ramírez-Angueta, J. Saüch-Pitarch, F. Ronzano, E. Centeno, F. Sanz, and L. I. Furlong, “The disgenet knowledge platform for disease genomics: 2019 update,” *Nucleic Acids Research*, vol. 48, p. D845–D855, 1 2020.
- [15] M. Karimi, D. Wu, Z. Wang, and Y. Shen, “Deepaffinity: interpretable deep learning of compound–protein affinity through unified recurrent and convolutional neural networks,” *Bioinformatics*, vol. 35, no. 18, pp. 3329–3338, 2019.
- [16] H. Öztürk, A. Özgür, and E. Ozkirimli, “Deepdta: deep drug–target binding affinity prediction,” *Bioinformatics*, vol. 34, no. 17, pp. i821–i829, 2018.
- [17] D. E. Gordon, G. M. Jang, M. Bouhaddou, J. Xu, K. Obernier, K. M. White, M. J. O’Meara, V. V. Rezelj, J. Z. Guo, D. L. Swaney, T. A. Tummino, R. Hüttenhain, R. M. Kaake, A. L. Richards, B. Tutuncuoglu, H. Foussard, J. Batra, K. Haas, M. Modak, M. Kim, P. Haas, B. J. Polacco, H. Braberg, J. M. Fabius, M. Eckhardt, M. Soucheray, M. J. Bennett, M. Cakir, M. J. McGregor, Q. Li, B. Meyer, F. Roesch, T. Vallet, A. M. Kain, L. Miorin, E. Moreno, Z. Z. C. Naing, Y. Zhou, S. Peng, Y. Shi, Z. Zhang, W. Shen, I. T. Kirby, J. E. Melnyk, J. S. Chorba, K. Lou, S. A. Dai, I. Barrio-Hernandez, D. Memon, C. Hernandez-Armenta, J. Lyu, C. J. P. Mathy, T. Perica, K. B. Pilla, S. J. Ganesan, D. J. Saltzberg, R. Rakesh, X. Liu, S. B. Rosenthal,

- L. Calviello, S. Venkataramanan, J. Liboy-Lugo, Y. Lin, X.-P. Huang, Y. Liu, S. A. Wankowicz, M. Bohn, M. Safari, F. S. Ugur, C. Koh, N. S. Savar, Q. D. Tran, D. Shengjuler, S. J. Fletcher, M. C. O’Neal, Y. Cai, J. C. J. Chang, D. J. Broadhurst, S. Klippsten, P. P. Sharp, N. A. Wenzell, D. Kuzuoglu-Ozturk, H.-Y. Wang, R. Trenker, J. M. Young, D. A. Cavero, J. Hiatt, T. L. Roth, U. Rathore, A. Subramanian, J. Noack, M. Hubert, R. M. Stroud, A. D. Frankel, O. S. Rosenberg, K. A. Verba, D. A. Agard, M. Ott, M. Emerman, N. Jura, M. von Zastrow, E. Verdin, A. Ashworth, O. Schwartz, C. d’Enfert, S. Mukherjee, M. Jacobson, H. S. Malik, D. G. Fujimori, T. Ideker, C. S. Craik, S. N. Floor, J. S. Fraser, J. D. Gross, A. Sali, B. L. Roth, D. Ruggero, J. Taunton, T. Kortemme, P. Beltrao, M. Vignuzzi, A. García-Sastre, K. M. Shokat, B. K. Shoichet, and N. J. Krogan, “A sars-cov-2 protein interaction map reveals targets for drug repurposing,” *Nature*, vol. 583, pp. 459–468, 2020.
- [18] S. M. Corsello^{1–3}, J. A. Bittker¹, Z. Liu¹, J. Gould¹, P. McCarren¹, J. E. Hirschman¹, S. E. Johnston¹, A. Vrcic¹, B. Wong¹, M. Khan¹, J. Asiedu¹, R. Narayan¹, C. C. Mader¹, A. Subramanian¹, and T. R. Golub, “The drug repurposing hub: a next-generation drug library and information resource,” *Nature Medicine*, vol. 23, no. 4, pp. 405–409, 2017.
- [19] D. He and L. Xie, “A cross-level information transmission network for hierarchical omics data integration and phenotype prediction from a new genotype,” *Bioinformatics*, 2021.
- [20] J. Mistry, S. Chuguransky, L. Williams, M. Qureshi, G. A. Salazar, E. L. Sonnhammer, S. C. Tosatto, L. Paladin, S. Raj, L. J. Richardson, *et al.*, “Pfam: The protein families database in 2021,” *Nucleic Acids Research*, vol. 49, no. D1, pp. D412–D419, 2021.
- [21] A. Gaulton, A. Hersey, M. Nowotka, A. P. Bento, J. Chambers, D. Mendez, P. Mutowo, F. Atkinson, L. J. Bellis, E. Cibrián-Uhalte, M. Davies, N. Dedman, A. Karlsson, M. P. Magariños, J. P. Overington, G. Papadatos, I. Smit, and A. R. Leach, “The ChEMBL database in 2017,” *Nucleic Acids Research*, vol. 45, pp. D945–D954, 11 2016.
- [22] H. Huang, G. Zhang, Y. Zhou, C. Lin, S. Chen, Y. Lin, S. Mai, and Z. Huang, “Reverse screening methods to search for the protein targets of chemopreventive compounds,” *Frontiers in chemistry*, vol. 6, p. 138, 2018.
- [23] O. Trott and A. J. Olson, “Autodock vina: improving the speed and accuracy of docking with a new scoring function, efficient optimization and multithreading,” *Journal of Computational Chemistry*, vol. 31, pp. 455–461, 2010.
- [24] S. Z. Grinter and X. Zou, “Challenges, applications, and recent advances of protein-ligand docking in structure-based drug design,” *Molecules*, vol. 19, no. 7, pp. 10150–10176, 2014.
- [25] M. Jaiteh, I. Rodríguez-Espigares, J. Selent, and J. Carlsson, “Performance of virtual screening against gpcr homology models: Impact of template selection and treatment of binding site plasticity,” *PLoS computational biology*, vol. 16, no. 3, p. e1007680, 2020.
- [26] S. M. Corsello, J. A. Bittker, Z. Liu, J. Gould, P. McCarren, J. E. Hirschman, S. E. Johnston, A. Vrcic, B. Wong, M. Khan, *et al.*, “The drug repurposing hub: a next-generation drug library and information resource,” *Nature medicine*, vol. 23, no. 4, pp. 405–408, 2017.
- [27] E. Barberis, V. V. Vanella, M. Falasca, V. Caneapero, G. Cappellano, D. Raineri, M. Ghirimoldi, V. D. Giorgis, C. Puricelli, R. Vaschetto, P. P. Sainaghi, S. Bruno, A. Sica, U. Dianzani, R. Rolla, A. Chiochetti, V. Cantaluppi, G. Baldanzi, E. Marengo, and M. Manfredi, “Circulating exosomes are strongly involved in sars-cov-2 infection,” *Front Mol Biosci* 8:632290, 2021.
- [28] C. Finan, A. Gaulton, F. A. Kruger, R. T. Lumbers, T. Shah, J. Engmann, L. Galver, R. Kelley, A. Karlsson, R. Santos, *et al.*, “The druggable genome and support for target identification and validation in drug development,” *Science translational medicine*, vol. 9, no. 383, 2017.
- [29] T. K. Sheils, S. L. Mathias, K. J. Kelleher, V. B. Siramshetty, D.-T. Nguyen, C. G. Bologa, L. J. Jensen, D. Vidović, A. Koleti, S. C. Schürer, A. Waller, J. J. Yang, J. Holmes, G. Bocci, N. Southall, P. Dharkar, E. Mathé, A. Simeonov, and T. I. Oprea, “Utrcd and pharos 2021: mining the human proteome for disease biology,” *Nucleic Acids Research*, vol. 49, pp. D1334–D1346, 1 2021.
- [30] C. Finan, A. Gaulton, F. A. Kruger, R. T. Lumbers, T. Shah, J. Engmann, L. Galver, R. Kelley, A. Karlsson, R. Santos, J. P. Overington, A. D. Hingorani, and J. P. Casas, “The druggable genome and support for target identification and validation in drug development,” *Science Translational Medicine*, vol. 9, p. eaag1166, 3 2017.

- [31] X. Jiao, B. T. Sherman, D. W. Huang, M. W. B. Robert Stephens, H. C. Lane, and R. A. Lempicki, “David-ws: a stateful web service to facilitate gene/protein list analysis,” *Bioinformatics*, vol. 28, p. 1805–1806, 7 2012.
- [32] D. O. Bates, J. C. Morris, S. Oltean, and L. F. Donaldson, “Pharmacology of modulators of alternative splicing,” *Pharmacological reviews*, vol. 69, no. 1, pp. 63–79, 2017.
- [33] K.-q. Le, B. S. Prabhakar, W.-j. Hong, and L.-c. Li, “Alternative splicing as a biomarker and potential target for drug discovery,” *Acta Pharmacologica Sinica*, vol. 36, no. 10, pp. 1212–1218, 2015.
- [34] J. E. Love, E. J. Hayden, and T. T. Rohn, “Alternative splicing in alzheimer’s disease,” *Journal of Parkinson’s disease and Alzheimer’s disease*, vol. 2, no. 2, 2015.
- [35] H. M. Berman, J. Westbrook, Z. Feng, G. Gilliland, T. N. Bhat, H. Weissig, I. N. Shindyalov, and P. E. Bourne, “The Protein Data Bank,” *Nucleic Acids Research*, vol. 28, pp. 235–242, 01 2000.
- [36] D. E. Gordon, G. M. Jang, M. Bouhaddou, J. Xu, K. Obernier, K. M. White, M. J. O’Meara, V. V. Rezelj, J. Z. Guo, D. L. Swaney, *et al.*, “A sars-cov-2 protein interaction map reveals targets for drug repurposing,” *Nature*, vol. 583, no. 7816, pp. 459–468, 2020.
- [37] I. Goodfellow, Y. Bengio, and A. Courville, *Deep Learning*. MIT Press, 2016. <http://www.deeplearningbook.org>.
- [38] H. Li, Z. Xu, G. Taylor, C. Studer, and T. Goldstein, “Visualizing the loss landscape of neural nets,” *arXiv preprint arXiv:1712.09913*, 2017.
- [39] P. Nakkiran, B. Neyshabur, and H. Sedghi, “The deep bootstrap: Good online learners are good offline generalizers,” *arXiv preprint arXiv:2010.08127*, 2020.
- [40] J.-Y. Le Boudec, *Performance evaluation of computer and communication systems*, vol. 2. Epfl Press Lausanne, 2010.
- [41] M. Arjovsky, “Out of distribution generalization in machine learning,” 2021.
- [42] M. Arjovsky, L. Bottou, I. Gulrajani, and D. Lopez-Paz, “Invariant risk minimization,” 2020.
- [43] A. D’Amour, K. Heller, D. Moldovan, B. Adlam, B. Alipanahi, A. Beutel, C. Chen, J. Deaton, J. Eisenstein, M. D. Hoffman, *et al.*, “Underspecification presents challenges for credibility in modern machine learning,” *arXiv preprint arXiv:2011.03395*, 2020.
- [44] V. Vapnik, “Principles of risk minimization for learning theory,” in *Advances in neural information processing systems*, pp. 831–838, 1992.
- [45] J. Yang, A. Roy, and Y. Zhang, “Biolip: a semi-manually curated database for biologically relevant ligand–protein interactions,” *Nucleic acids research*, vol. 41, no. D1, pp. D1096–D1103, 2012.
- [46] S. C. Potter, A. Luciani, S. R. Eddy, Y. Park, R. Lopez, and R. D. Finn, “Hmmer web server: 2018 update,” *Nucleic acids research*, vol. 46, no. W1, pp. W200–W204, 2018.
- [47] K. Xu, W. Hu, J. Leskovec, and S. Jegelka, “How powerful are graph neural networks?,” *arXiv preprint arXiv:1810.00826*, 2018.
- [48] S. Boyd and L. Vandenberghe, *Introduction to applied linear algebra: vectors, matrices, and least squares*. Cambridge university press, 2018.
- [49] C. d. Santos, M. Tan, B. Xiang, and B. Zhou, “Attentive pooling networks,” *arXiv preprint arXiv:1602.03609*, 2016.
- [50] K. He, X. Zhang, S. Ren, and J. Sun, “Deep residual learning for image recognition,” in *Proceedings of the IEEE conference on computer vision and pattern recognition*, pp. 770–778, 2016.
- [51] E. Rosenfeld, P. Ravikumar, and A. Risteski, “The risks of invariant risk minimization,” *arXiv preprint arXiv:2010.05761*, 2020.
- [52] K. Zhou, Z. Liu, Y. Qiao, T. Xiang, and C. C. Loy, “Domain generalization: A survey,” *arXiv preprint arXiv:2103.02503*, 2021.

- [53] K. Muandet, D. Balduzzi, and B. Schölkopf, “Domain generalization via invariant feature representation,” in *International Conference on Machine Learning*, pp. 10–18, PMLR, 2013.
- [54] B. Kulis, K. Saenko, and T. Darrell, “What you saw is not what you get: Domain adaptation using asymmetric kernel transforms,” in *CVPR 2011*, pp. 1785–1792, IEEE, 2011.
- [55] A. Ben-Tal, L. El Ghaoui, and A. Nemirovski, *Robust optimization*. Princeton university press, 2009.
- [56] H. Rahimian and S. Mehrotra, “Distributionally robust optimization: A review,” 2019.
- [57] W. Hu, G. Niu, I. Sato, and M. Sugiyama, “Does distributionally robust supervised learning give robust classifiers?,” in *International Conference on Machine Learning*, pp. 2029–2037, PMLR, 2018.
- [58] Y. Bengio, A. C. Courville, and P. Vincent, “Unsupervised feature learning and deep learning: A review and new perspectives,” *CoRR*, vol. abs/1206.5538, 2012.
- [59] K. Huang, T. Fu, L. M. Glass, M. Zitnik, C. Xiao, and J. Sun, “Deeppurpose: A deep learning library for drug-target interaction prediction,” *Bioinformatics*, 2020.
- [60] M. Eisenstein, “Active machine learning helps drug hunters tackle biology.,” *Nature biotechnology*, vol. 38, no. 5, pp. 512–515, 2020.
- [61] Y. Bengio, J. Louradour, R. Collobert, and J. Weston, “Curriculum learning,” in *Proceedings of the 26th annual international conference on machine learning*, pp. 41–48, 2009.
- [62] G. Koch, R. Zemel, and R. Salakhutdinov, “Siamese neural networks for one-shot image recognition,” in *ICML deep learning workshop*, vol. 2, Lille, 2015.

Contents

1	Introduction	2
2	Conceptual basis of Portal Learning	3
3	Results and Discussion	4
3.1	Overview of PortalCG	4
3.2	There are significantly unexplored dark spaces in chemical genomics	5
3.3	Portal Learning significantly outperforms state-of-the-art approaches to predicting dark CPIs	5
3.4	Both the STL and OOC-ML stages contribute to the improved performance of PortalCG	6
3.5	Application of PortalCG to explore dark chemical genomics space	6
3.5.1	COVID-19 polypharmacology	6
3.5.2	Illuminating the undruggable human genome	7
4	Conclusion	8
5	Methods	8
5.1	Full algorithm details	8
5.2	Data	9
5.3	Experiment implementation	9
5.4	Related works	9
	Author Contributions	15
	Data and software availability	15
	Acknowledgement	15
	Reference	16
A	Key terms	22
B	Methods: PortalCG in four-universe configuration for dark chemical genomics space	24
B.1	Data preprocessing	24
B.2	Algorithm	24
B.2.1	Chemical representation	24
B.2.2	Protein sequence pre-training	24
B.2.3	Protein structure regularization	24
B.2.4	Out-of-cluster Meta Learning (OOC-ML) in protein function universe	25
B.2.5	Stress model instance selection	26
B.3	Implementation details	26
B.4	Evaluation metrics	26
B.5	Docking as baseline	26
B.6	Production level for deployment	27
B.7	Dark space exploration from a theoretical lens	27
C	Additional tables	28
	Table S1: Drugs predicted to interact with SARS-COVID-2 interactors	28
	Table S2: Undruggable human disease-associated proteins selected by PortalCG	28
	Table S3: Chemicals interacted with undruggable human proteins	33
	Table S4: Functional Annotation enrichment for human proteins in Tbio selected by PortalCG	34
	Table S5: Top ranked diseases associated with proteins in Tbio selected by portal learning	35
	Table S6: Chemicals interacted with human proteins in Tbio	35
	Table S7: Functional Annotation enrichment for undruggable human disease proteins without Tbio selected by PortalCG	35
	Table S8: Top ranked diseases associated with undruggable human proteins excluding Tbio selected by portal learning	35
	Table S9: Chemicals interacted with undruggable human proteins excluding Tbio	35
	Table S10: Model architecture configuration	35
D	Related works	38
D.1	OOD generalization in deep learning	38
D.2	Portal learning key components related	38

E Additional figures	40
Figure S1: Dark space statistics histogram	40
Figure S2: Dark space statistics trend line	40
Figure S3: Dark space statistics heatmap	40
Figure S4: Model performance breakdown to each class	40
Figure S5: Model performance t-test	40
Figure S6: Stress model selection performance curves against DISAE as baseline	40
Figure S7: Model performance histogram	40
Figure S8: The binding conformations and 2D-interactions of Fenebrutinib on the targeted proteins predicted by using Autodock	40
Figure S9: The binding conformations and 2D-interactions of Fenebrutinib on the targeted proteins predicted by using Autodock	40
Figure S10: The binding conformations and 2D-interactions of NMS-P715 on the targeted proteins predicted by using Autodock	40
Figure S11: Histogram equalization results	40
Figure S12: Ablation study	40
Figure S13: Model architecture illustration	40

A Key terms

To provide common ground for discussion with readers of various backgrounds, we list the specification of key terms related to the methods in Supplemental materials. The following list provides explanations at an intuition level without the attempt to establish formal definitions. Readers could refer to referenced materials for more formal definitions.

Deep learning specific

1. model architecture: the design of a model as a set of trainable parameters without specification on the exact weight of the parameters [37].
2. loss landscape: the geometry of the global loss associated with a model architecture[38].
3. model instance: given a model architecture with certain amount of trainable parameters, a set of weights associated to the trainable parameters defines an instance of model; during the training process, each optimization step leads to a model instance.
4. optimization[37]: neural network is trained by optimizing a object function, usually in the form of minimizing a loss function.
5. global/local optimum: under the optimization formalization, the optimum point is at the end of the optimization process. As explained in [39], in an ideal world where the complete distribution of data is available to train a model, the optimum is global; while any stop point for any certain subdistribution is a local optimum.
6. model initialization: optimization always starts with an initialization of an model instance.
7. pretraining[10]: train a model on a pretext task before training on the target task; the trained model instances will become the initialization of the target task.
8. finetuning[10]: train a model on a target task with initialization pretrained task.
9. Independent and Identically distributed (IID)[40]: if given a set of data x_i , each of these x_i observations is an independent draw from a fixed (“stationary”) probability distribution.
10. Out-of-distribution (OOD) generalization[41]: Generalization consists in reducing the gap in performance between training data and testing data. When the data generating process from the training data is indistinguishable from that of the test data, it’s “in-distribution”, if not, it’s called out-of-distribution generalization problem [41]. As in [42], considering datasets $Data_e := \{(x_i^e, y_i^e)\}_{i=1}^{n_e}$ collected under multiple domains e , each containing samples IID with a probability distribution $D(X^e, Y^e)$. The goal of OOD generalization is to use these datasets to learn a predictor $Y \approx f(X)$, which performs well across a large set of unseen but related domains $e \in \mathcal{E}_{all}$. Namely, the goal is to minimize

$$R^{OOD}(f) = \max_{e \in \mathcal{E}_{all}} R^e(f) \quad (1)$$

, where

$$R^e(f) := E_{X^e, Y^e}[l(f(X^e), Y^e)] \quad (2)$$

is the risk under domain e . Here the set \mathcal{E}_{all} contains all possible domains.

11. generalization[37]: the most general goal of generalization is to enable the model make reliable prediction on unseen data; out-of-distribution prediction (OOD) is a more challenging type of generalization problem which requires the model to be generalizable to unseen data distribution.
12. mini-batch[37]: as a common practice for robustness and computation memory concerns, no matter how large a data set is available, only a sub set of data is sampled to train a model at each optimization step.
13. representation[37]: as coined by the line of work named “representation learning”, the word representation is interchangeable with “embedding”, referring to a vector/matrix of learned features.
14. transfer model parameter: a technique that is related to pretraining-finetuning; for the implementation, a simple initialization of part of the target model using the pretrained model could serve the purpose.

Chemical-protein interaction (CPI) specific

1. CPI prediction: formulated as a binary classification task, to predict whether or not a pair of protein and chemical will bind given only protein sequence and chemical SMILES string.
2. protein descriptor, chemical descriptor: the modules of a whole CPI prediction model to extract protein/chemical embedding in a euclidean space.

Portal learning specific

1. universe: a model architecture that defines a data transformation space, together with a data set.
2. portal: a model instance in a universe—which could be a local optimum in the current universe, but which facilitates moving the model to the global optimum in the ultimately targeted universe.
3. local loss landscape: optimize a model on a sub-distribution of the complete underlying distribution of the whole data set.
4. global loss landscape: the direction of gradient search towards global optimum for all sub-distributions.
5. stress test: a technique[43] to evaluate a predictor by observing its outputs on specifically designed inputs; three common types are stratified performance evaluation, shifted evaluation and contrastive evaluation.
6. shifted evaluation[43]: the stress test employed in this paper, which splits train/test data set by Pfam families, i.e. proteins in the testing and training sets come from different Pfam families. This is a simple simulation off dark space model deployment.
7. deployment gap: the difference between the performance evaluated by the test set and that evaluated by the development set.
8. classic deep learning training scheme: randomly split a whole data set into train/dev/test set; optimize model on a randomly sampled mini-batch data; choose a final trained model instance based on the best test evaluation metrics; usually adopts empirical risk minimization [44] formulation.

B Methods: PortalCG in four-universe configuration for dark chemical genomics space

In this section, we present the detailed methodology used in portal learning in the context of a four-universe configuration.

B.1 Data preprocessing

The four-universe configuration is built on three major databases, Pfam[20], Protein Data Bank (PDB)[35], BioLip[45] and ChEMBL[21]. The data were preprocessed as follows.

- Protein sequence universe. All sequences from Pfam-A families are used to pretrain the protein descriptor following the same setting in DISAE [1] that highlights a MSA-based distillation process.
- Protein structure universe. In our protein structure data set, there are 30,593 protein structures, 13,104 ligands, and 91,780 ligand binding sites. Binding sites were selected according to the annotation from BioLip (updated to the end of 2020). Binding sites which contact with DNA/RNA and metal ions were not included. If a protein has more than one ligand, multiple binding pockets were defined for this protein. For each binding pocket, the distances between $C\alpha$ atoms of amino acid residues of the binding pocket were calculated. In order to obtain the distances between the ligand and its surrounding binding site residues, the distances between atom i in the ligand and each atom in the residue j of the binding pocket were calculated and the smallest distance was selected as the distance between atom i and residue j . In order to get the sequence feature of the binding site residues in the DISAE protein sequence representation[1], binding site residues obtained from PDB structures (queries) were mapped onto the multiple sequence alignments of its corresponding Pfam family. First, a profile HMM database was built for the whole Pfam families. hmmscan [46] was applied to search the query sequence against this profile database to decide which Pfam family it belongs to. For those proteins with multiple domains, more than one Pfam families were identified. Then the query sequence was aligned to the most similar sequence in the corresponding Pfam family by using phmmer. Aligned residues on the query sequence were mapped to the multiple sequence alignments of this family according to the alignment between the query sequence and the most similar sequence.
- Chemical universe. All chemicals in the ChEMBL26 database consists of the chemical universe.
- Protein function universe. CPI classification prediction data is the whole ChEMBL26[21] database where the same threshold for defining positive and negative labels creating as that in DISAE [1] was used.

B.2 Algorithm

In the four-universe configuration, portal learning starts with portal identification in the protein sequence universe, then travels into protein structure universe for portal calibration before finally comes into the target protein function universe, where OOC-ML will be invoked for model optimization. Along the way, shifted evaluation, one type of stress model selection, is used to select the “best” model instance, which splits train/test based on Pfam families, i.e. training set and testing set have proteins come from different Pfam families. Each phase will be specified in the following sections.

B.2.1 Chemical representation

A chemical was represented as a graph and its embedding was learned using GIN[47].

B.2.2 Protein sequence pre-training

Protein descriptor is pretrained from scratch following exactly DISAE [1] on whole Pfam families, making it a universal protein language model. With standard Adam optimization, shifted evaluation is used to select the “best” instance.

B.2.3 Protein structure regularization

With the protein descriptor pretrained using the sequences from the whole Pfam, chemical descriptors and a distance learner were plugged in to fine-tune the protein representation. The distance learner follows AlphaFold[4] which formulates a multi-way classification on a distrogram. Based on the

histogram of binding site distances, a histogram equalization¹ was applied to formulate a 10-way classification on our binding site structure data as in Supplemental material Figure S S11. Since protein and chemical descriptors output position-specific embeddings of a distilled protein sequence and all atoms of a chemical, pair-wise interaction features on the binding sites were created with a simple vector operation: a matrix multiplication was used to select embedding vectors of each binding residue and atom; multiply and broadcast the selected embedding vectors into a symmetric tensor as shown in the following, where H is embedding matrix of size $(number_of_residues, embedding_dimension)$ or $(number_of_atoms, embedding_dimension)$ and A is selector matrix[48],

$$\begin{aligned} H_{binding_site}^{protein} &= A^{protein} * H_{full_distilled}^{protein} \\ H_{binding_site}^{chemical} &= A^{chemical} * H_{full_chemical_graph}^{chemical} \\ H_{binding_site}^{interaction} &= (H_{binding_site}^{protein})^T * H_{binding_site}^{chemical} \end{aligned}$$

This pair-wise interaction feature tensor $H_{binding_site}^{interaction}$ was fed into a Attentive Pooling[49] layer followed by feed-forward layer for final 10-way classification. Detailed model architecture configuration could be found in Table S S10 and Figure SS13. The intuition for the simplest form of distance learner is to put all stress of learning on the shared protein and chemical descriptors which will carry information across universes. Again, with standard Adam optimization, shifted evaluation was used to select the “best” instance. Two versions of distance structure prediction were implemented, one formulated as a binary classification, i.e. contact prediction, one formulated as a multi-way classification, i.e. distogram prediction. The performance of the two version are similar, as shown in Figure S S12.

B.2.4 Out-of-cluster Meta Learning (OOC-ML) in protein function universe

With fine-tuned protein descriptor in the protein function universe, a binary classifier is plugged on, which is a ResNet[50] layered with two linear layers as shown in Table S S10 and Figure SS13. What plays the major role in this phase is the optimization algorithm OOC-ML as shown in pseudocode **Algorithm1** and main content Figure 1(B),(C.1). The local loss landscape exploration is reflected in line 4-9, and line 10 shows ensemble of global loss landscape. Note that more variants could be derived from changing sampling rule (line 3 and 5) and global loss ensemble rule.

OOC-ML is built on MAML[11] but has significant differences. Echoing to steps illustrated in the Figure 1 of the main text:

1. As shown in main content Figure1 (B), OOC-ML has a sub-distribution data split into support set and query set, or as MAML named it, meta-train and meta-test within training set and test set. However, MAML sub-distributions are identified from the label space $\{Y\}$ while OOC-ML identifies sub-distributions, i.e. clusters, from input feature space $\{X\}$. In PortalCG, the clusters are identified by Pfam. Further, OOC-ML allows the utilization of very small clusters where very limited known data points are available for training. For example, in PortalCG, some Pfam families with too few samples to be split into support and query set are organized as query-set-alone, which participate only in the global loss optimization, as detailed below.
2. In each mini-batch, a few sub-distributions are sampled. The whole optimization has two layers, inner loop and outer loop. At the inner loop, each sub-distribution data has its own local loss landscape. The support set is used for in-distribution optimization on the local loss landscape.
3. The locally optimized model is then used on query set to get a query set loss, which will be fed to the global loss landscape. Each sub-distribution is independently optimized. This step is the same as MAML. What is different is that OOC-ML also calculates query-set without local in-distribution optimization for the small clusters.
4. Local query set losses are pooled together and the model will be optimized on the global loss landscape as meta-optimization defined in MAML.
5. After finishing train, the model will be deployed.
6. MAML is designed for multi-class classification in few-shot learning, at deployment stage, it’s expected to meet new unseen class. And it’s assumed that there are **a few labelled sample available** as support set, hence named as **few-shot learning**. For each unseen class, the trained model will carry out a fast in-distribution adaptation using support set before final prediction on the query set. However, this is impossible in the context of dark space illumination. Portal learning trained model has to make robust predictions without any chance of in-distribution adaptation.

¹Histogram equalization: https://en.wikipedia.org/wiki/Histogram_equalization

Algorithm 1: Portal Learning Optimization Algorithm: Out-of-cluster Meta-learning

input : $p(\mathbf{D})$, CPI data distribution over whole pfams, where each $D_i \in \mathbf{D}$ is a set of CPI pairs for the $pfam_i$;
 α, β , learning step size hyperparameters;
 L , number of optimization steps in each round of local exploration;
 T , number of global training steps;
 K , number of points sampled from a local neighborhood

output: θ the whole model weights

- 1 initialization whole model weights θ (with weight transferred from portal for protein and chemical descriptors and random initialized weights for binary classifier)
- 2 **for** t *in* T **do**
- 3 Sample a $D_i \sim p(D)$;
- 4 **for** l *in* L **do**
- 5 Sample a positive-negative balanced mini-batch of K pairs $neighborhood_m \sim D_i$;
- 6 **for** $point_j$ *in* $neighborhood_m$ **do**
- 7 Evaluate $\nabla_{\theta} L_{point_j}(f_{\theta})$ with respect to K examples;
- 8 Compute adapted parameters with gradient decent: $\theta'_i = \theta - \alpha \nabla_{\theta} L_{point_j}(f_{\theta})$;
- 9 **end**
- 10 Update $\theta \leftarrow \theta - \beta \nabla_{\theta} \sum_{D_i \sim p(D)} L_{point_j}(f'_{\theta})$;
- 11 **end**
- 12 **end**

B.2.5 Stress model instance selection

In classic training scheme common practice, there are 3-split data sets, “train set”, “dev set” and “test set”. Train set as the name suggested is used to train model. Test set as commonly expected is used to set an expectation of performance when applying the trained model to unseen data. Dev set is to select the preferred model instance. In OOD setting, data is split (main content Table 1) such that dev set is a OOD from train set and test set is a OOD from both train and dev set. Deployment gap is calculated by deducting ODD-dev performance with OOD-test performance.

B.3 Implementation details

With portal learning being a framework, all experiments are based on the configuration of a four-universe design. Four major variants of models are trained as shown in main content Table 2 for controlled factor experiments to verify the contribution of key components of Portal Learning. In this section we present implementation details.

Due to the large number of total samples, all training are carried out under global step-based formalization instead of epoch-based. Typically, a deep learning model is trained for numerous epochs, in each epoch the model will loop over all training data. Evaluation will be carried out once on the whole test data set at the end of each epoch. In the global step formalization, a mini-batch is sampled at uniform random from pre-split training data set. For a pre-defined total number of global steps, this mini-batch sampling will be repeated. Training is stopped when loss decreases are within a pre-defined error margin. To evaluate along the way of training, for every m global steps of training, a subset of test data is sampled uniformly randomly from a pre-split test set. To compute generalization gaps, in addition to evaluate on test set split according to the shifted evaluation, a dev set is held out from the train set for the evaluation as well. In this way, dev set and train set are iid. The performance difference between dev and train is the *observed space generalization gap* while the performance difference between dev and test is the *dark space generalization gap*.

B.4 Evaluation metrics

Distogram prediction uses an average accuracy on the distogram. CPI binary classification uses F1, ROC-AUC and PR-AUC for overall evaluation with breakdown by class F1, recall and precision scores.

B.5 Docking as baseline

Protein-ligand docking was performed using Autodock Vina[23]. The whole protein surface search implemented in the Autodock Vina was applied to identify the ligand binding pocket. The center of each protein was set as the center of the binding pocket. The largest distance of the protein atoms to the center of the protein is calculated for each x, y, and z direction to define the edge of each

protein. 10 Angstrom of extra space was added to the protein edge to set up the search space for the docking.

B.6 Production level for deployment

To create a production level model, three models were trained in PortalCG with only difference in data split. Dev set was OOD in respect of training set to make sure there was no overlapped Pfam families between them. By rotating Pfam families between training set and OOD-dev set in the fashion of a cross-validation, each of the three models was trained on different train set in light of Pfam families involved. Then a voting mechanism was used to make the final prediction.

B.7 Dark space exploration from a theoretical lens

A neural network classifier is trained by minimizing a loss function with a standard form as the following:

$$L(\theta) = \frac{1}{|D_t|} \sum_{(x,y) \in D_t} -\log p_\theta(x, y)$$

where $p_\theta(x, y)$ is the probability that a sample x belongs to the class y according to the trained neural network with parameters θ , and D_t is the training data set with the number of samples $|D_t|$. As laid out in the recent framework in [39] that reasons about generalization in deep learning, the test error of a model f_t could be decomposed as follows,

$$TestError(f_t) = \underbrace{TestError(f_t^{iid})}_{\text{ideal world}} + \underbrace{[TestError(f_t) - TestError(f_t^{iid})]}_{\text{real world generalization gap}}$$

When data are sampled as independent and identically distributed (iid) random variables, “ideal world” is a scenario where the complete data distribution is available with infinite data and optimization is on a population loss landscape. By contrast, “real world” has only finite data, where optimization is on an empirical loss landscape. In the dark space context of the OOD setting, this decomposition needs to be changed to

$$TestError(f_t^{OOD}) = \underbrace{TestError(f_t^{iid})}_{\text{observed space}} + \underbrace{[TestError(f_t^{OOD}) - TestError(f_t^{iid})]}_{\text{dark space generalization gap}}$$

and

$$TestError(f_t^{iid}) = TrainError(f_t^{iid}) + \underbrace{[TestError(f_t^{iid}) - TrainError(f_t^{iid})]}_{\text{observed space generalization gap}}$$

This explains that the effort could be devoted to decrease the observed space error and/or the dark space generalization gap to reduce $TestError(f_t^{OOD})$.

$$\begin{aligned} \nabla_\theta J(\theta) &\approx g = \frac{1}{m} \sum_{i=1}^m \nabla_\theta L(x^{(i)}, y^{(i)}, \theta) \\ \theta &\leftarrow \theta - \epsilon g \end{aligned}$$

When stochastic gradient descent (SDG) is applied to the optimization, it approximately estimates $\nabla_\theta J(\theta)$, the expectation of gradient, using a small set of sample of size m , i.e., the mini-batch drawn uniformly from the training set. When all data are IID, this approximation works fine to update θ with g . However, for the OOD with unknown distribution, this θ updating function could easily fall into a local minimum based on the m mini-batch samples.

The test error for a trained model in the OOD setting includes two parts: test errors in the observed IID space and a generalization gap when stepping into the OOD space. Furthermore, as discussed and proved in [41], [42], not all OOD tasks are equal. Depending on how different the OOD data set is from the train set, some OOD task could be more challenge. It is true for predicting ligand binding to dark proteins. It is impossible for training data to provide sufficient coverage of the whole distribution in the dark chemical genomics space. The motivation of Portal Learning for exploring the dark space follows: one model architecture defines a functional mapping space, together with a data set defines a **universe**. The model initialized instance in a universe closer to the global optimum universe is a **portal** that is transferred from an associated universe. CPI dark space is impossible to be explored if the learning is confined only in the observed protein function, i.e. CPI universe since the known data are far sparse as shown in main content Figure 3. Hence STL is important to identify portals. The model optimization on a loss function can decrease IID training errors but will not help with the observed IID space generalization gap $TestError(f_t)^{iid} - TrainError(f_t^{iid})$ or the dark space generalization gap $TestError(f_t^{OOD}) - TestError(f_t^{iid})$. With Portal Learning, stress model instance selection can narrow the first gap and OOC-ML can narrow the second gap.

C Additional tables

Uniprot	Protein name	Drug name	Probscore	
WNEODWDFDXWOLU-QHCPKHFHSA-N	7	fenebrutinib	phase 2	Bruton's tyrosine kinase (BTK) inhibitor
JFOAJUGFHDCEBJJ-UHFFFAOYSA-N	7	NMS-P715	preclinical	protein kinase inhibitor
QHLVBKQYJGBCQJ-UHFFFAOYSA-N	4	NMS-1286937	phase 2	PLK inhibitor
FUXVKZWTXQUGMW-FQEVSTJZSA-N	4	9-aminocamptothecin	phase 2	topoisomerase inhibitor
DKZYXHCYPUVGAF-JCNLHEQBSA-N	2	OTS167	phase 1/phase 2	maternal embryonic leucine zipper kinase inhibitor
VYLOOGHLKSNNEK-PIIMJCKOSA-N	1	tropifexor	phase 2	FXR agonist
TZKBVRDEOITLRB-UHFFFAOYSA-N	1	GZD824	preclinical	Bcr-Abl kinase inhibitor
KZSKGLFYQAYZCO-UHFFFAOYSA-N	1	cilofexor	phase 3	FXR agonist

Table S1: Drugs predicted to interact with SARS-COVID-2 interactors

Uniprot	Protein name	Drug name	Probscore
Q8TEX9	Importin-4	fenebrutinib	0.68089414
Q8NB66	Protein unc-13 homolog C	AI-10-49	0.67951804
Q9NZF1	Placenta-specific gene 8 protein	AI-10-49	0.6778485
Q96G03	Phosphoglucomutase-2	fenebrutinib	0.677423
Q8IWU4	Zinc transporter 8	fenebrutinib	0.677423
P53004	Biliverdin reductase A	AI-10-49	0.6769635
P40879	Chloride anion exchanger	fenebrutinib	0.67688245
Q8IYL2	Probable tRNA	fenebrutinib	0.6768823
Q9ULL4	Plexin-B3	AI-10-49	0.67652583
Q96SZ6	Mitochondrial tRNA methyltransferase CDK5RAP1	fenebrutinib	0.6763639
Q9BRT9	DNA replication complex GINS protein SLD5	fenebrutinib	0.6763639
Q8N2U0	Transmembrane protein 256	CCT137690	0.67634773
Q9UC06	Zinc finger protein 70	fenebrutinib	0.6761195
Q9BPX5	Actin-related protein 2/3 complex subunit 5-like protein	Q-203	0.67571765
Q8TDF6	RAS guanyl-releasing protein 4	NMS-1286937	0.6756182
Q9P2G3	Kelch-like protein 14	NMS-1286937	0.6756182
Q9HBT7	Zinc finger protein 287	CCT137690	0.6752016
Q9UKR8	Tetraspanin-16	PF-05190457	0.6751168
P59044	NACHT, LRR and PYD domains-containing protein 6	MK-5046	0.67498016
Q16774	Guanylate kinase	MK-5046	0.6749801
Q9HCE5	N6-adenosine-methyltransferase non-catalytic subunit	PF-05190457	0.67497396
Q15185	Prostaglandin E synthase 3	cilofexor	0.6745854
Q8WUA7	TBC1 domain family member 22A	fenebrutinib	0.67439413
Q17RS7	Flap endonuclease GEN homolog 1	CGM097	0.67434615
Q14244	Enscosin	PF-05190457	0.67431164
Q9BRK5	45 kDa calcium-binding protein	PF-05190457	0.67431164
Q9UKJ5	Cysteine-rich hydrophobic domain-containing protein 2	CCT137690	0.67429835
Q6ZWJ1	Syntaxin-binding protein 4	AI-10-49	0.6742442
Q9HAR2	Adhesion G protein-coupled receptor L3	AI-10-49	0.67414063
P98161	Polycystin-1	AI-10-49	0.67414063
Q92673	Sortilin-related receptor	AI-10-49	0.6740716
D6RGH6	Multicilin	fenebrutinib	0.67397785
Q8NHH9	Atlastin-2	fenebrutinib	0.67395777
Q9H0E2	Toll-interacting protein	PF-05190457	0.6739072
O15145	Actin-related protein 2/3 complex subunit 3	PF-05190457	0.6739072
P51116	Fragile X mental retardation syndrome-related protein 2	abemaciclib	0.6738332
Q9BR09	Neutralized-like protein 2	elbasvir	0.67369795
P42568	Protein AF-9	AI-10-49	0.67364717
P17600	Synapsin-1	AI-10-49	0.67364717
P48553	Trafficking protein particle complex subunit 10	AI-10-49	0.6736086
Q12955	Ankyrin-3	abemaciclib	0.6735056

Table S2 continued from previous page

Uniprot	Protein name	Drug name	Probscore
O60936	Nucleolar protein 3	abemaciclib	0.6735056
Q02575	Helix-loop-helix protein 1	AI-10-49	0.6734969
P49640	Homeobox even-skipped homolog protein 1	CFI-402257	0.67348343
P22670	MHC class II regulatory factor RFX1	PF-05190457	0.67346805
Q8IUF8	Ribosomal oxygenase 2	NMS-1286937	0.67343307
P22681	E3 ubiquitin-protein ligase CBL	NMS-1286937	0.67343307
Q7RTS3	Pancreas transcription factor 1 subunit alpha	MK-5046	0.67334837
Q9Y5L4	Mitochondrial import inner membrane translocase subunit Tim13	NMS-P715	0.6733338
P17735	Tyrosine aminotransferase	PF-05190457	0.673238
O95294	RasGAP-activating-like protein 1	PF-05190457	0.673224
Q8NCD3	Holliday junction recognition protein	PF-05190457	0.673224
Q86W28	NACHT, LRR and PYD domains-containing protein 8	MK-5046	0.6731598
Q04671	P protein	AI-10-49	0.67310166
Q9C035	Tripartite motif-containing protein 5	AI-10-49	0.6731016
Q66K64	DDB1- and CUL4-associated factor 15	AI-10-49	0.672944
Q5T9A4	ATPase family AAA domain-containing protein 3B	CFI-402257	0.67286545
Q96MP8	BTB/POZ domain-containing protein KCTD7	CFI-402257	0.6728654
Q9UIE0	Zinc finger protein 230	CFI-402257	0.672853
Q3SYG4	Protein PTHB1	abemaciclib	0.67280704
Q8IUY3	GRAM domain-containing protein 2A	AI-10-49	0.67273754
O75689	Arf-GAP with dual PH domain-containing protein 1	AI-10-49	0.67273754
Q9NZP8	Complement C1r subcomponent-like protein	fenebrutinib	0.6727066
Q9NQX4	Unconventional myosin-Vc	fenebrutinib	0.6727064
Q15388	Mitochondrial import receptor subunit TOM20 homolog	CFI-402257	0.6726911
Q9NXL9	DNA helicase MCM9	piperaquine-phosphate	0.6726752
P53370	Nucleoside diphosphate-linked moiety X motif 6	piperaquine-phosphate	0.6726752
Q8N7C0	Leucine-rich repeat-containing protein 52	PF-05190457	0.67262363
O95231	Homeobox protein VENTX	NMS-P715	0.67261267
Q9HC56	Protocadherin-9	AI-10-49	0.6725752
A6NNW6	Enolase 4	AI-10-49	0.6725752
P35612	Beta-adducin	CFI-402257	0.67255336
Q9Y6M5	Zinc transporter 1	AI-10-49	0.67255074
Q01804	OTU domain-containing protein 4	AI-10-49	0.6725507
Q9Y678	Coatomer subunit gamma-1	MK-5046	0.67254347
Q9BTY7	Protein HGH1 homolog	AI-10-49	0.67243195
Q8NEM0	Microcephalin	CFI-402257	0.6724283
Q7LGA3	Heparan sulfate 2-O-sulfotransferase 1	AI-10-49	0.67242616
O75956	Cyclin-dependent kinase 2-associated protein 2	ziritaxestat	0.6723895
P62987	Ubiquitin-60S ribosomal protein L40	ziritaxestat	0.6723893
Q14257	Reticulocalbin-2	CDK9-IN-6	0.6723883
Q9H0I3	Coiled-coil domain-containing protein 113	tropifexor	0.6723477
P32019	Type II inositol 1,4,5-trisphosphate 5-phosphatase	fenebrutinib	0.6723469
O95409	Zinc finger protein ZIC 2	fenebrutinib	0.6723469
P56179	Homeobox protein DLX-6	fenebrutinib	0.67233485
Q12798	Centrin-1	AI-10-49	0.6722851
Q14714	Sarcospan	AI-10-49	0.6722851
Q96LI5	CCR4-NOT transcription complex subunit 6-like	abemaciclib	0.6722749

Table S2 continued from previous page

Uniprot	Protein name	Drug name	Probscore
Q86XR7	TIR domain-containing adapter molecule 2	AI-10-49	0.6722719
P53672	Beta-crystallin A2	CCT137690	0.6722543
O43439	Protein CBFA2T2	CCT137690	0.6722543
Q9H0E3	Histone deacetylase complex subunit SAP130	fenebrutinib	0.6722474
Q8NFZ0	F-box DNA helicase 1	fenebrutinib	0.6722474
Q8N0S2	Synaptonemal complex central element protein 1	CFI-402257	0.67223567
Q92667	A-kinase anchor protein 1, mitochondrial	fenebrutinib	0.67222863
O60884	DnaJ homolog subfamily A member 2	PF-05190457	0.6721347
P41214	Eukaryotic translation initiation factor 2D	AI-10-49	0.6721203
Q6R327	Rapamycin-insensitive companion of mTOR	AI-10-49	0.67211396
O75886	Signal transducing adapter molecule 2	PF-05190457	0.67206836
Q9UMX6	Guanylyl cyclase-activating protein 2	PF-05190457	0.6720683
Q99447	Ethanolamine-phosphate cytidylyltransferase	CCT137690	0.67205685
Q6FI13	Histone H2A type 2-A	PF-05190457	0.6720233
Q969S2	Endonuclease 8-like 2	fenebrutinib	0.67200994
Q6XZF7	Dynamin-binding protein	AI-10-49	0.67196065
Q96EX1	Small integral membrane protein 12	fenebrutinib	0.6719141
Q8TD57	Dynein axonemal heavy chain 3	fenebrutinib	0.6719141
O15375	Monocarboxylate transporter 6	PF-05190457	0.6719058
Q9H7E2	Tudor domain-containing protein 3	NMS-1286937	0.6718896
A6NI73	Leukocyte immunoglobulin-like receptor subfamily A member 5	AI-10-49	0.671879
Q9NZM3	Intersectin-2	CDK9-IN-6	0.6718554
O75145	Liprin-alpha-3	CDK9-IN-6	0.6718554
Q9NSD9	Phenylalanine-tRNA ligase beta subunit	abemaciclib	0.6718319
O15195	Villin-like protein	abemaciclib	0.6718319
P05538	HLA class II histocompatibility antigen, DQ beta 2 chain	cilofexor	0.671822
Q8TD57	Dynein axonemal heavy chain 3	cilofexor	0.671822
Q9NRD9	Dual oxidase 1	abemaciclib	0.6718094
Q8WUQ7	Cactin	AI-10-49	0.67178315
Q9H7C4	Syncoilin	AI-10-49	0.67178315
Q70EK9	Ubiquitin carboxyl-terminal hydrolase 51	PF-05190457	0.671742
O43837	Isocitrate dehydrogenase [NAD] subunit beta, mitochondrial	PF-05190457	0.67174196
Q9UKY1	Zinc fingers and homeoboxes protein 1	CFI-402257	0.6717407
Q6ZMJ2	Scavenger receptor class A member 5	CFI-402257	0.6717407
P61371	Insulin gene enhancer protein ISL-1	fenebrutinib	0.6717256
Q6NSZ9	Zinc finger and SCAN domain-containing protein 25	fenebrutinib	0.6717256
Q92754	Transcription factor AP-2 gamma	IACS-10759	0.67171496
Q5RKV6	Exosome complex component MTR3	AI-10-49	0.6716919
Q9BRA0	N-alpha-acetyltransferase 38, NatC auxiliary subunit	MK-5046	0.6716785
Q9BSF8	BTB/POZ domain-containing protein 10	CCT137690	0.67165
Q6PJ69	Tripartite motif-containing protein 65	AI-10-49	0.6716369
Q9NRP0	Oligosaccharyltransferase complex subunit OSTC	AI-10-49	0.6716369
Q8TBM7	Transmembrane protein 254	PF-05190457	0.6716311
Q674X7	Kazrin	elbasvir	0.6716015
Q9Y3C4	EKC/KEOPS complex subunit TPRKB	abemaciclib	0.6715913
P59190	Ras-related protein Rab-15	abemaciclib	0.6715913
Q9NZM3	Intersectin-2	PF-05190457	0.6715465
P05455	Lupus La protein	AI-10-49	0.6715072
Q96KN3	Homeobox protein PKNOX2	abemaciclib	0.67148525

Table S2 continued from previous page

Uniprot	Protein name	Drug name	Probscore
P54278	Mismatch repair endonuclease PMS2	abemaciclib	0.6714852
P49069	Guided entry of tail-anchored proteins factor CAMLG	fenebrutinib	0.6714454
Q8IYT4	Katanin p60 ATPase-containing subunit A-like 2	AI-10-49	0.6714413
Q8WV10	Small integral membrane protein 4	AI-10-49	0.67144126
Q9Y6X6	Unconventional myosin-XVI	MK-5046	0.6713607
Q8N357	Solute carrier family 35 member F6	MK-5046	0.6713607
Q96BP2	Coiled-coil-helix-coiled-coil-helix domain-containing protein 1	abemaciclib	0.671357
Q9UJQ4	Sal-like protein 4	MK-5046	0.67135173
Q9HCQ5	Polypeptide N-acetylgalactosaminyltransferase 9	fenebrutinib	0.67132807
Q9P2Q2	FERM domain-containing protein 4A	fenebrutinib	0.67132807
Q7Z7M8	UDP-GlcNAc:betaGal beta-1,3-N-acetylglucosaminyltransferase 8	NMS-P715	0.6713157
Q9HCK5	Protein argonaute-4	PF-05190457	0.6713007
O95405	Zinc finger FYVE domain-containing protein 9	AI-10-49	0.67127687
Q92911	Sodium/iodide cotransporter	PF-05190457	0.67127484
Q8WWI1	LIM domain only protein 7	fenebrutinib	0.6712641
Q8N3C7	CAP-Gly domain-containing linker protein 4	fenebrutinib	0.671264
Q9UBS8	E3 ubiquitin-protein ligase RNF14	PF-05190457	0.671259
Q9BY66	Lysine-specific demethylase 5D	PF-05190457	0.671259
Q9UPM8	AP-4 complex subunit epsilon-1	abemaciclib	0.6712124
Q9BYE0	Transcription factor HES-7	MK-5046	0.6711568
Q9BSD7	Cancer-related nucleoside-triphosphatase	AI-10-49	0.67114973
Q9NXH9	tRNA	tropifexor	0.6711371
Q13948	Protein CASP	tropifexor	0.6711371
Q9C019	Tripartite motif-containing protein 15	abemaciclib	0.67111254
Q5TA50	Ceramide-1-phosphate transfer protein	ABT-702	0.6711099
Q7KZF4	Staphylococcal nuclease domain-containing protein 1	ABT-702	0.6711099
P08247	Synaptophysin	fenebrutinib	0.6711092
A4IF30	Solute carrier family 35 member F4	AI-10-49	0.67109805
Q9NRA8	Eukaryotic translation initiation factor 4E transporter	AI-10-49	0.67109805
Q96FF9	Sororin	acalabrutinib	0.6710895
P10073	Zinc finger and SCAN domain-containing protein 22	PF-05190457	0.67107534
P0CW19	LIM and senescent cell antigen-like-containing domain protein 3	PF-05190457	0.67107534
Q9UPM8	AP-4 complex subunit epsilon-1	fenebrutinib	0.6710706
P08118	Beta-microseminoprotein	PF-05190457	0.6710468
Q96P16	Regulation of nuclear pre-mRNA domain-containing protein 1A	fenebrutinib	0.6710315
P62280	40S ribosomal protein S11	piperaquine-phosphate	0.6710226
Q8TE49	OTU domain-containing protein 7A	AI-10-49	0.6710194
Q53HI1	Protein unc-50 homolog	AI-10-49	0.6710194
Q8WW32	High mobility group protein B4	PF-05190457	0.6709929
P57729	Ras-related protein Rab-38	PF-05190457	0.67099285
Q8N2M8	CLK4-associating serine/arginine rich protein	fenebrutinib	0.6709883
P25705	ATP synthase subunit alpha, mitochondrial	fenebrutinib	0.6709781
Q9Y5H3	Protocadherin gamma-A10	PF-05190457	0.6709645
Q9NU63	Zinc finger protein 57 homolog	fenebrutinib	0.67096215
P43363	Melanoma-associated antigen 10	AI-10-49	0.6709133

Table S2 continued from previous page

Uniprot	Protein name	Drug name	Probscore
Q13469	Nuclear factor of activated T-cells, cytoplasmic 2	AI-10-49	0.670904
Q8NG77	Olfactory receptor 2T12	AI-10-49	0.670904
Q9Y2G8	DnaJ homolog subfamily C member 16	PF-05190457	0.67090386
Q9ULV8	E3 ubiquitin-protein ligase CBL-C	fenebrutinib	0.67089945
Q96EF0	Myotubularin-related protein 8	elbasvir	0.67085487
Q8TD16	Protein bicaudal D homolog 2	abemaciclib	0.6708334
P49459	Ubiquitin-conjugating enzyme E2 A	abemaciclib	0.6708334
Q6XZF7	Dynamin-binding protein	AI-10-49	0.6708271
Q9Y4I1	Unconventional myosin-Va	AI-10-49	0.6708271
Q96FL9	Polypeptide N-acetylgalactosaminyltransferase 14	MK-5046	0.67080116
Q9HD67	Unconventional myosin-X	MK-5046	0.6708011
Q13214	Semaphorin-3B	MK-5046	0.6707926
Q53H47	Histone-lysine N-methyltransferase SETMAR	MK-5046	0.6707926
P46776	60S ribosomal protein L27a	AI-10-49	0.67078424
Q15306	Interferon regulatory factor 4	AI-10-49	0.6707842
Q2TAA2	Isoamyl acetate-hydrolyzing esterase 1 homolog	abemaciclib	0.67076474
O43324	Eukaryotic translation elongation factor 1 epsilon-1	PF-05190457	0.67074585
Q96R27	Olfactory receptor 2M4	fenebrutinib	0.6707435
Q5VXU1	Sodium/potassium-transporting ATPase subunit beta-1-interacting protein 2	fenebrutinib	0.6707435
Q5VWQ8	Disabled homolog 2-interacting protein	fenebrutinib	0.67072076
Q9UJF2	Ras GTPase-activating protein nGAP	elbasvir	0.67071134
O75923	Dysferlin	fenebrutinib	0.6707069
O75592	E3 ubiquitin-protein ligase MYCBP2	PF-05190457	0.6706958
Q14714	Sarcospan	CFI-402257	0.67069536
Q12798	Centrin-1	CFI-402257	0.67069536
Q9H9Z2	Protein lin-28 homolog A	fenebrutinib	0.67065567
Q8N2A8	Mitochondrial cardiolipin hydrolase	fenebrutinib	0.67065555
Q5VV41	Rho guanine nucleotide exchange factor 16	abemaciclib	0.6706521
Q96QT6	PHD finger protein 12	fenebrutinib	0.67064524
Q13948	Protein CASP	AI-10-49	0.6706354
Q9NXH9	tRNA	AI-10-49	0.6706354
Q969E2	Secretory carrier-associated membrane protein 4	fenebrutinib	0.67062545
P58107	Epiplakin	fenebrutinib	0.67062545
P55036	26S proteasome non-ATPase regulatory subunit 4	NMS-P715	0.67059726
Q11128	4-galactosyl-N-acetylglucosaminide 3-alpha-L-fucosyltransferase FUT5	AI-10-49	0.6705861
Q86W28	NACHT, LRR and PYD domains-containing protein 8	AI-10-49	0.6705852
O43566	Regulator of G-protein signaling 14	Q-203	0.67055416
Q9BVI0	PHD finger protein 20	Q-203	0.67055416
Q93074	Mediator of RNA polymerase II transcription subunit 12	PF-05190457	0.67054135
P51530	DNA replication ATP-dependent helicase/nuclease DNA2	PF-05190457	0.6705413
Q6NS38	DNA oxidative demethylase ALKBH2	AI-10-49	0.67052937
B4DJY2	Transmembrane protein 233	AI-10-49	0.67052513
Q8N807	Protein disulfide-isomerase-like protein of the testis	PF-05190457	0.67051905
P13929	Beta-enolase	AI-10-49	0.67051786
Q9NRJ7	Protocadherin beta-16	AI-10-49	0.67051774
O95751	Protein LDOC1	MK-5046	0.67051023

Table S2 continued from previous page

Uniprot	Protein name	Drug name	Probscore
Q92947	Glutaryl-CoA dehydrogenase, mitochondrial	fenebrutinib	0.67050344
Q96J94	Piwi-like protein 1	fenebrutinib	0.6704877
O15400	Syntaxin-7	adapalene	0.67046946
O00192	Armadillo repeat protein deleted in velo-cardio-facial syndrome	adapalene	0.67046934
Q17RD7	Synaptotagmin-16	CFI-402257	0.6704517
A0PJZ3	Glucoside xylosyltransferase 2	MK-5046	0.67042667
Q53GG5	PDZ and LIM domain protein 3	PF-05190457	0.6704057
P20929	Nebulin	PF-05190457	0.6704056
Q5NDL2	EGF domain-specific O-linked N-acetylglucosamine transferase	abemaciclib	0.67039376
Q10570	Cleavage and polyadenylation specificity factor subunit 1	fenebrutinib	0.6703786
Q53FE4	Uncharacterized protein C4orf17	AI-10-49	0.67036396
Q96T21	Selenocysteine insertion sequence-binding protein 2	cilofexor	0.67036384
P17980	26S proteasome regulatory subunit 6A	PF-05190457	0.67036086
Q8TE77	Protein phosphatase Slingshot homolog 3	tropifexor	0.67035466
Q96LD4	E3 ubiquitin-protein ligase TRIM47	tropifexor	0.67035466
P25205	DNA replication licensing factor MCM3	fenebrutinib	0.6703515
Q9NQC7	Ubiquitin carboxyl-terminal hydrolase CYLD	fenebrutinib	0.6703515
Q71F23	Centromere protein U	NMS-P715	0.6703202
P46778	60S ribosomal protein L21	fenebrutinib	0.67028475
Q04727	Transducin-like enhancer protein 4	AI-10-49	0.6702773
O14556	Glyceraldehyde-3-phosphate dehydrogenase, testis-specific	AI-10-49	0.6702773
Q92994	Transcription factor IIIB 90 kDa subunit	fenebrutinib	0.67027074
Q15646	2'-5'-oligoadenylate synthase-like protein	fenebrutinib	0.67027074
O15131	Importin subunit alpha-6	fenebrutinib	0.6702412
Q14254	Flotillin-2	fenebrutinib	0.6702412
O75764	Transcription elongation factor A protein 3	CFI-402257	0.67017365
P40425	Pre-B-cell leukemia transcription factor 2	MK-5046	0.67016166
O43766	Lipoyl synthase, mitochondrial	PF-05190457	0.67014426
Q969L2	Protein MAL2	fenebrutinib	0.67013794
Q9NSG2	Uncharacterized protein C1orf112	CCT137690	0.67013377
Q9H892	Tetratricopeptide repeat protein 12	PF-05190457	0.67012644
O95248	Myotubularin-related protein 5	CCT137690	0.6701216
O60481	Zinc finger protein ZIC 3	PF-05190457	0.670091
Q9UBK8	Methionine synthase reductase	AI-10-49	0.6700795
Q4G0J3	La-related protein 7	CCT137690	0.67007875
Q8WW32	High mobility group protein B4	CCT137690	0.67005986
P23297	Protein S100-A1	MK-5046	0.67002577
Q8TCB7	tRNA N	elbasvir	0.6700179
Q8IXH6	Tumor protein p53-inducible nuclear protein 2	abemaciclib	0.67000955

Table S2: Undruggable human disease-associated proteins selected by ProtalCG

When we consider the proteins in Tbio, there are 9545 proteins which are not in Casas's druggable proteins. If 0.67 was used as the cutoff, 219 proteins were predicted as positive hits. The gene enrichment analysis result for these proteins was listed in Table SS4. Disease associated with these 219 human proteins were also listed in Table SS5. Since one protein is always related with multiple diseases, these diseases are ranked by the number of their associated proteins and the top 10 diseases were listed in the table. Most of top ranked diseases are related with cancer development. 21 drugs that are approved or in clinical trial are predicted to interact with these proteins as shown in Table SS6.

If the proteins in Tbio were removed from the undruggable list, only 2930 proteins were left.

Drug name	Clinical phase	Mechanism of Action	Number of targeted proteins
AI-10-49	Preclinical	core binding factor inhibitor	63
Fenebrutinib	Phase 2	Bruton's tyrosine kinase (BTK) inhibitor	56
PF-05190457	Phase 2	growth hormone secretagogue receptor inverse agonist	42
Abemaciclib	Launched	CDK inhibitor	21
MK-5046	Preclinical	bombesin receptor agonist	18
CFI-402257	Phase 1/Phase 2	dual specificity protein kinase inhibitor	14
CCT137690	Preclinical	Aurora kinase inhibitor	11
Tropifexor	Phase 2	FXR agonist	5
NMS-1286937	Phase 2	PLK inhibitor	5
NMS-P715	Preclinical	protein kinase inhibitor	5
Elbasvir	Launched	HCV inhibitor	5
Cilofexor	Phase 3	FXR agonist	4
CDK9-IN-6	Preclinical	CDK inhibitor	3
piperazine-phosphate	Launched	antimalarial agent	3
Q-203	Phase 2	ATP synthase inhibitor	3
ABT 702 dihydrochloride	Preclinical	adenosine kinase inhibitor	2
Ziritaxestat	Phase 3	autotaxin inhibitor	2
Adapalene	Launched	retinoid receptor agonist	1
Acalabrutinib	Launched	Bruton's tyrosine kinase (BTK) inhibitor	1
IACS-10759 Hydrochloride	Preclinical	mitochondrial complex I inhibitor	1
NVP-CGM097	Phase 1	MDM inhibitor	1

Table S3: Chemicals interacted with undruggable human proteins

If 0.67 was used as the cutoff, there will be only 41 proteins predicted positive and no significant enrichment with David gene enrichment analysis. So 0.665 was used as a cutoff, and 348 proteins were predicted as positive hits. The gene enrichment analysis result for these proteins was listed in Table SS7. Disease associated with these 348 human proteins were also listed in Table SS8. 42 drugs that are approved or in clinical trial are predicted to interact with these proteins as shown in Table SS9.

David Functional Annotation enrichment analysis				
Enriched terms in UniProtKB keywords	Number of proteins involved	Percentage of proteins involved	P-value	Modified Benjamini p-value
Alternative splicing	153	69.9	2.70E-08	6.80E-06
Phosphoprotein	126	57.5	1.70E-07	2.20E-05
Cytoplasm	82	37.4	3.20E-06	2.40E-04
Nucleus	87	39.7	3.70E-06	2.40E-04
Metal-binding	61	27.9	2.00E-04	1.00E-02

Table S4: Functional Annotation enrichment for human proteins in Tbio selected by PortalCG

Disease Name	# of undruggable proteins associated with the disease
Breast Carcinoma	89
Tumor Cell Invasion	85
Carcinogenesis	83
Neoplasm Metastasis	73
Colorectal Carcinoma	68
Liver carcinoma	66
Non-Small Cell Lung Carcinoma	56
Malignant neoplasm of lung	56
Carcinoma of lung	54
Alzheimer's Disease	54

Table S5: Top ranked diseases associated with proteins in Tbio selected by portal learning

rug name	Clinical phase	Mechanism of Action	Number of targeted proteins
AI-10-49	Preclinical	core binding factor inhibitor	52
fenebrutinib	Phase 2	Bruton's tyrosine kinase (BTK) inhibitor	45
PF-05190457	Phase 2	growth hormone secretagogue receptor inverse agonist	36
abemaciclib	Launched	CDK inhibitor	20
MK-5046	Preclinical	bombesin receptor agonist	15
CFI-402257	Phase 1/Phase 2	dual specificity protein kinase inhibitor	14
CCT137690	Preclinical	Aurora kinase inhibitor	7
NMS-1286937	Phase 2	PLK inhibitor	5
tropifexor	Phase 2	FXR agonist	4
NMS-P715	Preclinical	protein kinase inhibitor	4
cilofexor	Phase 3	FXR agonist	3
CDK9-IN-6	Preclinical	CDK inhibitor	3
piperazine-phosphate	Launched	antimalarial agent	3
elbasvir	Launched	HCV inhibitor	3
ABT-702	Preclinical	adenosine kinase inhibitor	2
adapalene	Launched	retinoid receptor agonist	2
Q-203	Phase 2	ATP synthase inhibitor	2
ziritaxestat	Phase 3	autotaxin inhibitor	2
acalabrutinib	Launched	Bruton's tyrosine kinase (BTK) inhibitor	1
IACS-10759	Preclinical	mitochondrial complex I inhibitor	1
CGM097	Phase 1	MDM inhibitor	1

Table S6: Chemicals interacted with human proteins in Tbio

David Functional Annotation enrichment analysis				
Enriched terms in UniProtKB keyword	Number of proteins involved	Percentage of proteins involved (%)	P-value	Modified Benjamini p-value
Zinc-finger	80	23	7.60E-16	1.20E-13
Zinc	85	24.4	1.20E-11	9.90E-10
Metal-binding	96	27.6	4.30E-06	2.30E-04
DNA-binding	62	17.8	7.90E-06	3.20E-04
Transcription regulation	61	17.5	5.60E-04	1.80E-02
Transcription	61	17.5	1.10E-03	3.00E-02

Table S7: Functional Annotation enrichment for undruggable human disease proteins without Tbio selected by PortalCG

Disease Name	# of undruggable proteins associated with the disease
Body Height	31
Colorectal Carcinoma	28
Malignant neoplasm of breast	26
Breast Carcinoma	18
Blood Protein Measurement	18
Leukemia, Myelocytic, Acute	17
Carcinogenesis	17
Neoplasm Metastasis	17
Liver carcinoma	15
Malignant neoplasm of prostate	15

Table S8: Top ranked diseases associated with undruggable human proteins excluding Tbio selected by portal learning

Drug_name	Clinical phase	Mechanism of Action	Number of targeted proteins
fenebrutinib	Phase 2	Bruton's tyrosine kinase (BTK) inhibitor	80
PF-05190457	Phase 2	growth hormone secretagogue receptor inverse agonist	50
MK-5046	Preclinical	bombesin receptor agonist	38
CCT137690	Preclinical	Aurora kinase inhibitor	36
AI-10-49	Preclinical	core binding factor inhibitor	31
abemaciclib	Launched	CDK inhibitor	26
CFI-402257	Phase 1/Phase 2	dual specificity protein kinase inhibitor	20
NMS-P715	Preclinical	protein kinase inhibitor	14
NMS-1286937	Phase 2	PLK inhibitor	11
elbasvir	Launched	HCV inhibitor	8
cilofexor	Phase 3	FXR agonist	7
ABBV-744	Phase 1	bromodomain inhibitor	7
tropifexor	Phase 2	FXR agonist	7
CDK9-IN-6	Preclinical	CDK inhibitor	6
adapalene	Launched	retinoid receptor agonist	4
Q-203	Phase 2	ATP synthase inhibitor	4
PLX8394	Phase 1/Phase 2	serine/threonine kinase inhibitor	4
ABT-702	Preclinical	adenosine kinase inhibitor	4
NVP-BSK805	Preclinical	JAK inhibitor	3
OTS167	Phase 1/Phase 2	maternal embryonic leucine zipper kinase inhibitor	3
CHIR-99021	Preclinical	glycogen synthase kinase inhibitor	3
DBPR-211	Preclinical	cannabinoid receptor antagonist	2
A-887826	Preclinical	sodium channel blocker	2
integrin-antagonist-1	Phase 1	integrin antagonist	2
piperazine-phosphate	Launched	antimalarial agent	2
cenerimod	Phase 2	sphingosine 1-phosphate receptor modulator	1
peposertib	Phase 1/Phase 2	DNA dependent protein kinase inhibitor	1
tezacaftor	Launched	CFTR channel agonist	1
cot-inhibitor-2	Preclinical	MAPK-interacting kinase inhibitor	1
itacitinib	Phase 3	JAK inhibitor	1
10-hydroxycamptothecin	Preclinical	topoisomerase inhibitor	1
alectinib	Launched	ALK tyrosine kinase receptor inhibitor	1
adarotene	Phase 1	retinoid receptor agonist	1
acalabrutinib	Launched	Bruton's tyrosine kinase (BTK) inhibitor	1
XL041	Preclinical	LXR agonist	1
WAY-207024	Preclinical	gonadotropin releasing factor hormone receptor antagonist	1
MK-5108	Phase 1	Aurora kinase inhibitor	1
CGM097	Phase 1	MDM inhibitor	1
CD-437	Preclinical	retinoid receptor agonist	1
AMG-925	Phase 1	CDK inhibitor/FLT3 inhibitor	1
ACT-132577	Launched	endothelin receptor antagonist	1
ziritaxestat	Phase 3	autotaxin inhibitor	1

Table S9: Chemicals interacted with undruggable human proteins excluding Tbio

Protein descriptor	layers	Albert ->Resnet
	embedding dimension	256
Chemical descriptor	backbone	GIN
	number of layers	5
	embedding dimension	300
	aggregation methods	sum
	drop out ratio	0.5
Interaction learner	layers	Attentive pooling ->2 layers of MLP
	embedding dimension	128
Structure residue-atom pair wise feature learner	layers	matrix multiplication of protein and chemical embedding vectors
Classifier	layers	2 layers of MLP
	embedding dimension	64

Table S10: Model architecture configuration

D Related works

D.1 OOD generalization in deep learning

The recent work Invariant risk minimization (IRM)[42] is a dedicated algorithm to OOD generalization, which is under the goal of transformative solution for invariant representation. However, given its completeness in theory, many experiments [51] report IRM are not doing well in large real-world data set.

Many deep learning tasks are inherently OOD generalization. Among those jargon, some are famous for defining a type of OOD scenario problem, for example, Domain generalization [52] can be taken as the equivalent of OOD generalization; domain shift [52] rephrases the fact of distribution change in terms of $D(X, y)$. Some jargon define a type of solution: domain alignment [53] minimizes the difference/distance between source domains and target domains distributions for an invariant representation where the distance between source and target domain distributions are measured by a wide variety of statistical distance metrics from simple l_2 , $f - divergence$ to Wasserstein distance; domain adaptation [54] is to leverage pretrained model on a different domain and is just one idea to achieve domain generalization, the more general term that is equivalent to OOD generalization in a more practical sense; causal learning is proved by [41] to be equivalent to OOD generalization when causality makes senses (taking into consideration the existence of cases where causality is meaningless); robust optimization [55] that focuses on worst-group performance instead of the average one in ERM; although robust optimization has not quite been adapted to modern deep learning, its sub-field distributional robust optimization [56] has witnessed quite a few recent works adapted to be used in deep learning.

Worth to be clarified that, many works that are solving the sub-group or sub-population shift problem is quite different from the OOD generalization problem as discussed in the setting of dark chemical genomics space. Sub-population shift is more like a imbalanced data problem where the test set has major resemblance with training data just the shift from a major class to a minor class or vice-versa. For example, GroupDRO [57] was published in 2018 to address this problem, proposing to incorporate structural assumptions on distribution, which could be straight forward in some data sets which has more meta-data or is a multi-label classification case where the label structure could be used as the structural assumption.

D.2 Portal learning key components related

(*Model architecture*) Even since the debut of the survey [58] enlightening the perspective of *representation learning*, enormous research passion is motivated for model architecture design, almost taken as equivalent to deep learning and overshadowing all other directions. A key idea that echos the demand of generalization is to learn *global representation* which helps to decrease both $TrainError(f_t^{iid})$ and *known space generalization gap*, denoising large data set. Hence, to solve OOD, good model architecture design is not enough.

All existing work in CPI is confined in the known space and limited works have concerned generalization. Generally, proposed CPI deep learning models follow the same fashion: build model architecture of three key modules, protein descriptor, chemical descriptor and interaction learner formulating a classification problem with a few variants as regression problem. Innovation is seen mostly for model architecture, particularly active for chemical descriptor, reflecting all milestones in recent years deep learning advancement from CNN, LSTM to Transformer and GNN as demonstrated in DeepPurpose [59]. Generalization has not shown in any previous work as a main goal of research except for DISAE[1] which proves generalizability to orphan GPCR protein drug screening mainly relying on a general purpose pretrained protein language model. It's fine-tuned on GPCR data set with shifted evaluation. Hence, DISAE becomes the baseline model in this work.

(*Model initialization*) Although could be categorized as a type of representation learning, *transfer learning* became an iconic independent concept for its huge success with breakthroughs in many NLP and CV benchmark tasks. It features a *pretraining-finetuning* procedure. An intuitive example is to pretrain a language model on large general English vocabulary with pretext task formulation such as predicting next word and then to finetune the language model on specific downstream task such as machine translation in biology domain. Well-renowned Transformer based pretrained models starting from human language models are a combined success of attention based model architecture design and transfer learning. In the computation biology field, most eye-catching equivalent is protein language model, i.e. protein descripto, which inspired several similar works at the same time by different groups: TAPE and ESM showcases pretraining on large protein vocabulary could significantly improves downstream task such as protein-protein interaction prediction; MSA-based-transformer and DISAE incorporates MSA in pretraining. From the perspective of the target downstream task, the power of transfer learning comes from a better model initialization. This is a major breakthrough that could fill the gap of $TestError(f_t^{OOD}) - TestError(f_t^{iid})$ but not

necessarily, depending on how it’s incorporated into the whole training scheme at system level, particularly depending on data fed in.

DISAE is used in our work here as a pretrained protein descriptor. This choice over other protein language models is due to the fact that DISAE is the smallest among other in terms of memory required to use and optimize with same level of performance. STL is a way to leverage transfer learning to fine better model initialization. The main difference and innovation is that transfer learning naively relies on the belief that more general knowledge transferred will bring better performance while STL in portal learning actively leverage biology endorsed biased when transferring general knowledge. Further, by defining the goal “to learn the portal”, which will be closer to global optimum in target universe loss landscape, the whole training system is steered actively solve ODD.

(*STL*) Sparked by the breakthrough of AlphaFold 1 [4] and AlphaFold 2[5] in protein structure prediction, deep learning has been trusted in molecule interaction distance map prediction to learn structure information. The inclusion of CPI-structure, i.e. protein function prediction portal calibration is inspired by recent success in protein structure prediction led by the great work of AlphaFold1[4] and AlphaFold2[5]. Specifically, we pretrain the model to predict residue-residue contacts for a protein whose structure is solved and chemical atom-protein residue contacts given a known CPI complex structure. There are three popular ways of residue-residue pairwise distance matrix prediction depending on how to formulate it as a machine learning task. On the one end is to formulate it as a binary classification where a distance threshold is set defining whether a pair of residues are in contact or not, hence the name contact prediction. On the other end is to formulate it as a regression problem where the exact distance is used as a regression target, hence the name exact distance prediction. AlphaFold1 showed another way in between the two ends, which is to formulate it as a multi-class classification problem, where the distribution of pair-wise residue distances is broken down into multiple class labels according to a histogram, hence the name distogram prediction. We first focus on residue-atom pair wise distance at binding sites and then experiments contact prediction and distogram prediction. In our results, the two formulations have similar performance in light of the final CPI prediction through ablation study as shown in Supplemental Figure SS12.

(*OOC-ML*) It’s long be aware that the sequence order of training data exposed to the model has an impact on model generalizability. Active learning [60] emphasises to actively query data in a iterative fashion to only expose the model to data close to he decision boundary . Curriculum learning [61] emphasises to sort all training so that the model is exposed to challenges of increasing difficulty. This element of data logistics has also been closely weaved into many optimization algorithms that aim to improve model generalizability. For example, contrastive loss[62] requires certain ratio of positive v.s. negative samples in each mini-bath. Most related to portal learning is meta-learning which can be categorized into metric-based, model-based and optimizer based “learn to learn” algorithms [12] with application to few-shot learning and zero-shot learning. Meta-learning started for the data-efficiency challenge instead of generalization or OOD. Although meta-learning is defined very general, making many algorithms seem to be mere an variants falling under its umbrella, in practice, algorithms proposed bearing the name of meta-learning are defined on multi-class classification data set, typically image classification, where the main challenge is the huge number of classes while limited data points are known in each class. Because of this underlying motivation, meta-learning features a very involving data logistics with multiple layer of optimization each has its meta-train/meta-test set sampled based on label distribution. These unspecified facts reveal that there is no existing meta-learning algorithm fit into CPI data.

However, the idea of “learn to learn” is attractive. MAML[11] is the optimization based meta-learning work that inspired OOC-ML proposed as a major component of portal learning. The differences are major. OOC-ML algorithm expands on it by focusing on data feature distribution instead of label distribution, encouraging active sampling in local neighborhood, which simplifies the support/query meta-train/meta-test data logistics, and ensembling a few local loss directions to learn global gravity direction.

E Additional figures

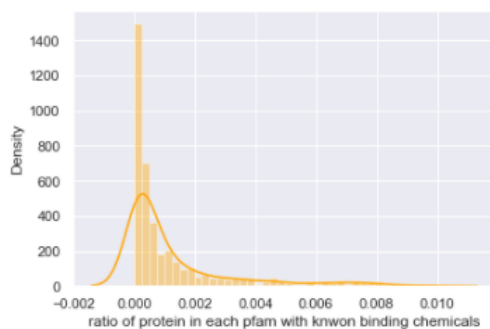


Figure S1: Dark space statistics histogram based on known CPI pairs in ChEMBL26. $< 1\%$ proteins in each pfam involved in ChEMBL26 have known binding chemicals.

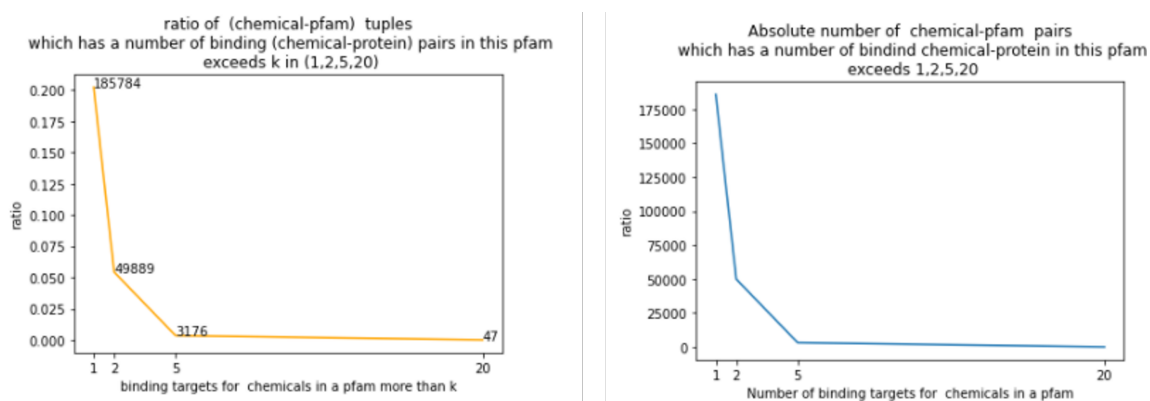


Figure S2: Dark space statistics histogram based on known CPI pairs in ChEMBL26. $< 1\%$ chemicals bind to more than 2 proteins; $< 0.4\%$ chemicals bind to more than 5 proteins.

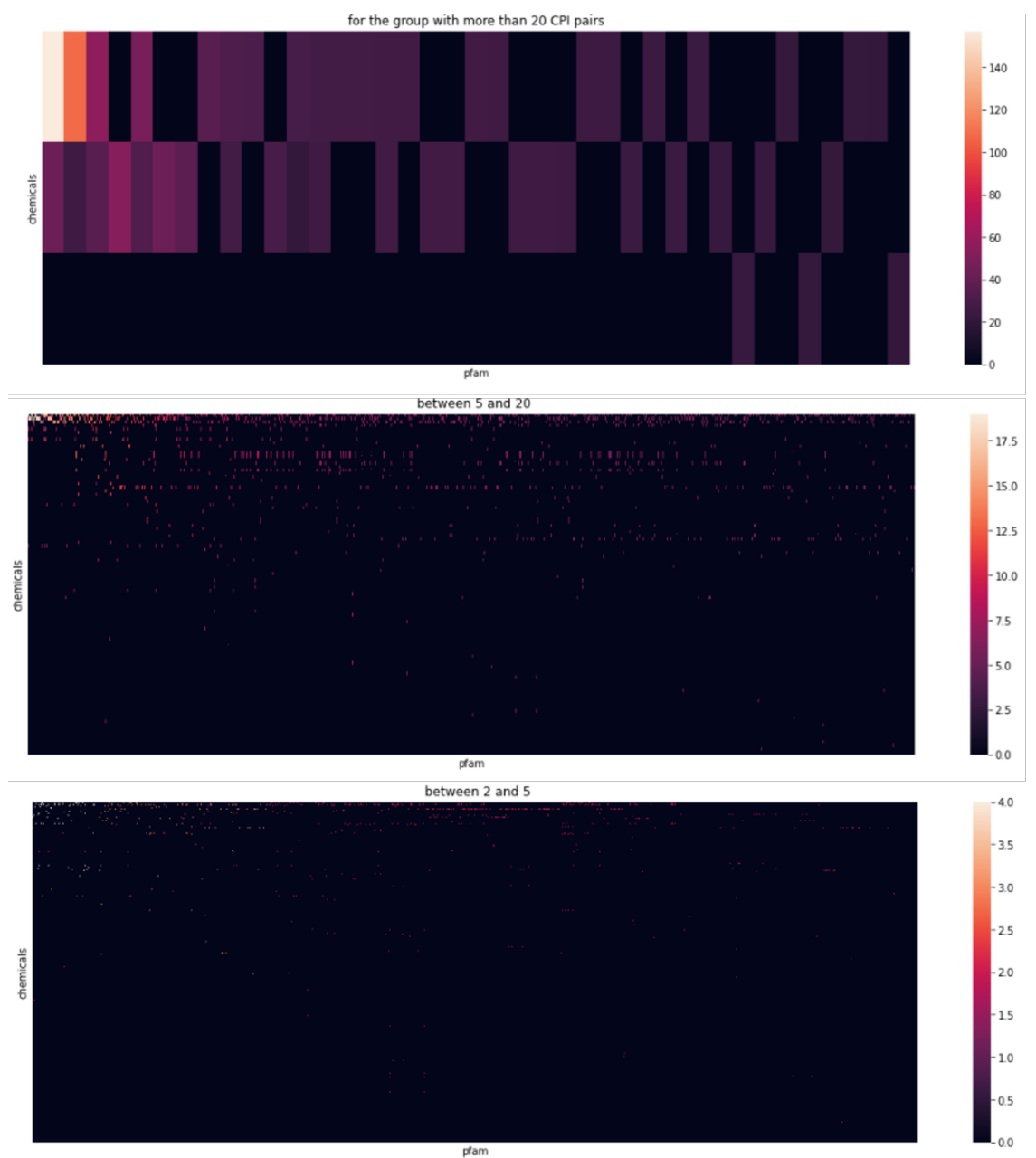


Figure S3: As shown in Figure S S2, there are three main ranges in terms of the binding targets in a pfam for one chemical: $[2,5]$, $[5,20]$, $[20,)$. For each of the range, a heatmap is shown with y axis representing each chemicals, x axis representing each pfam, each point representing the known binding pairs for one chemical and one pfam. As we can see, there is huge dark space.

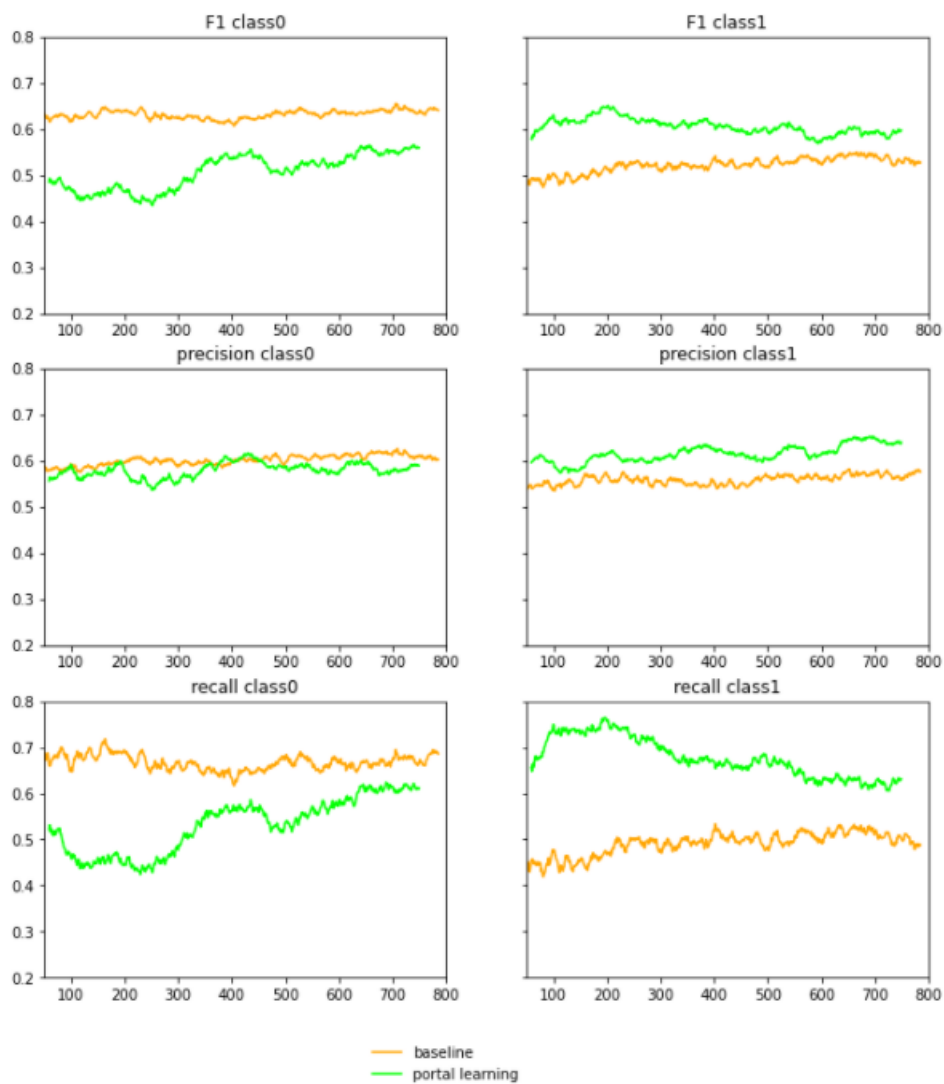


Figure S4: In the main text, overall evaluation across positive and negative classes are reported, such as F1, ROC-AUC, PR-AUC. Here is a breakdown of performance in each class, where class0 is negative, i.e. not binding, class1 is positive, i.e. binding, against DISAE as baseline

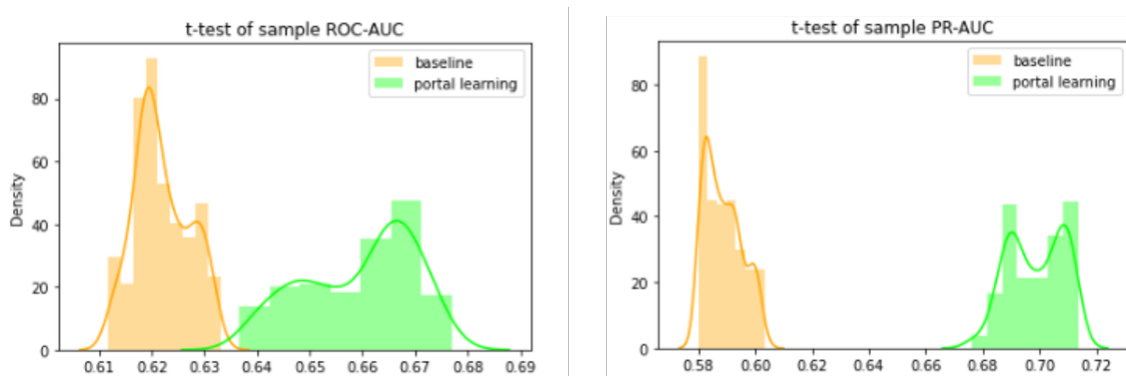


Figure S5: t-test comparison. The p-values for both ROC-AUC and PR-AUC are close to 0 against DISAE as baseline

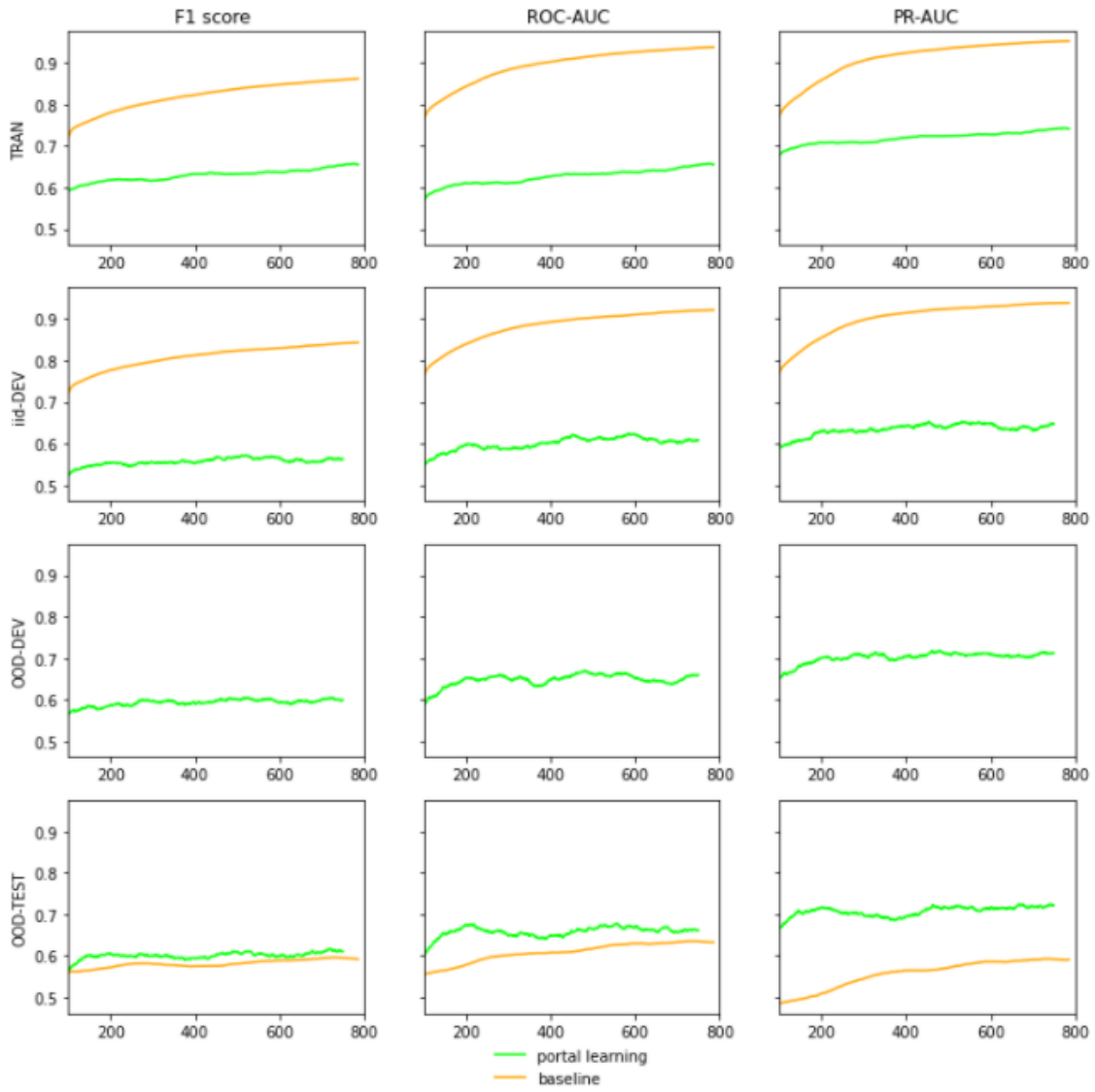


Figure S6: Stress model selection performance curves against DISAE as baseline

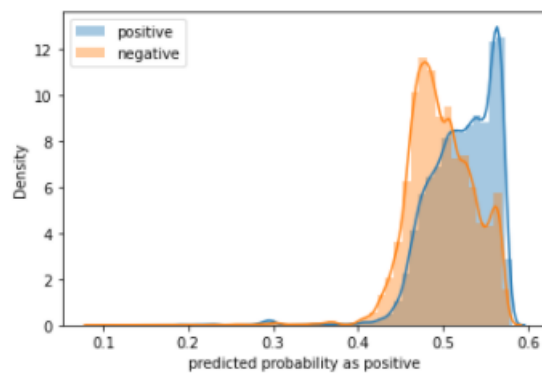
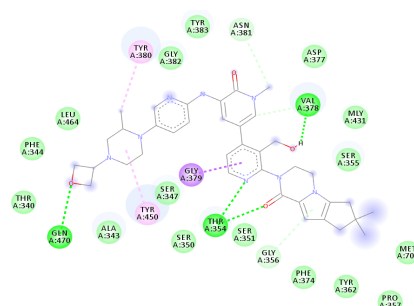
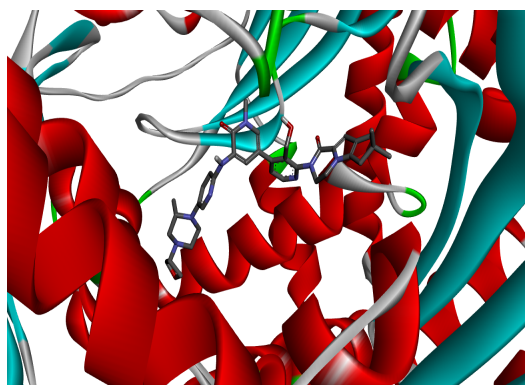


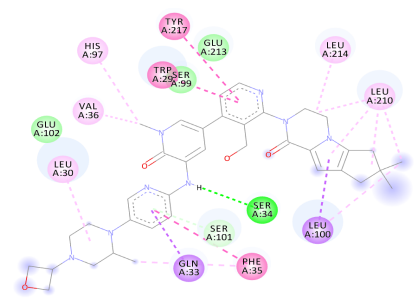
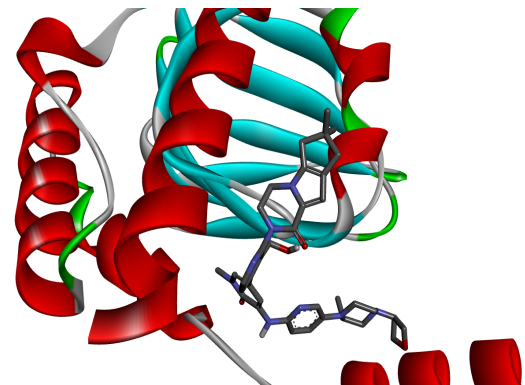
Figure S7: To select high confidence prediction, one additional procedure of filtering is to build a histogram of prediction scores based on known pairs. A threshold of 0.67 is identified to filter out confident positive prediction.



Interactions

- van der Waals
- Conventional Hydrogen Bond
- Pi-Donor Hydrogen Bond
- Pi-Sigma
- Pi-Alkyl

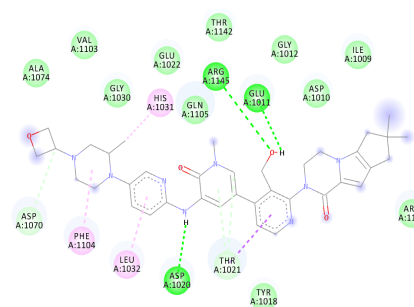
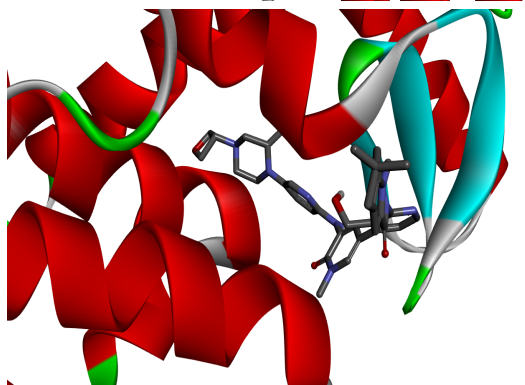
(a)



Interactions

- van der Waals
- Conventional Hydrogen Bond
- Pi-Donor Hydrogen Bond
- Pi-Sigma
- Pi-Pi Stacked
- Pi-Pi T-shaped
- Alkyl
- Pi-Alkyl

(b)



Interactions

- van der Waals
- Conventional Hydrogen Bond
- Pi-Donor Hydrogen Bond
- Pi-Sigma
- Pi-Alkyl

(c)

Figure S8: The binding conformations and 2D-interactions of Fenebutrinib on the targeted proteins predicted by using Autodock: (a) Fenebutrinib on Presequence protease. (b) Fenebutrinib on Sigma non-opioid intracellular receptor 1 . (c) Fenebutrinib on Mitochondrial amidoxime-reducing component 1.

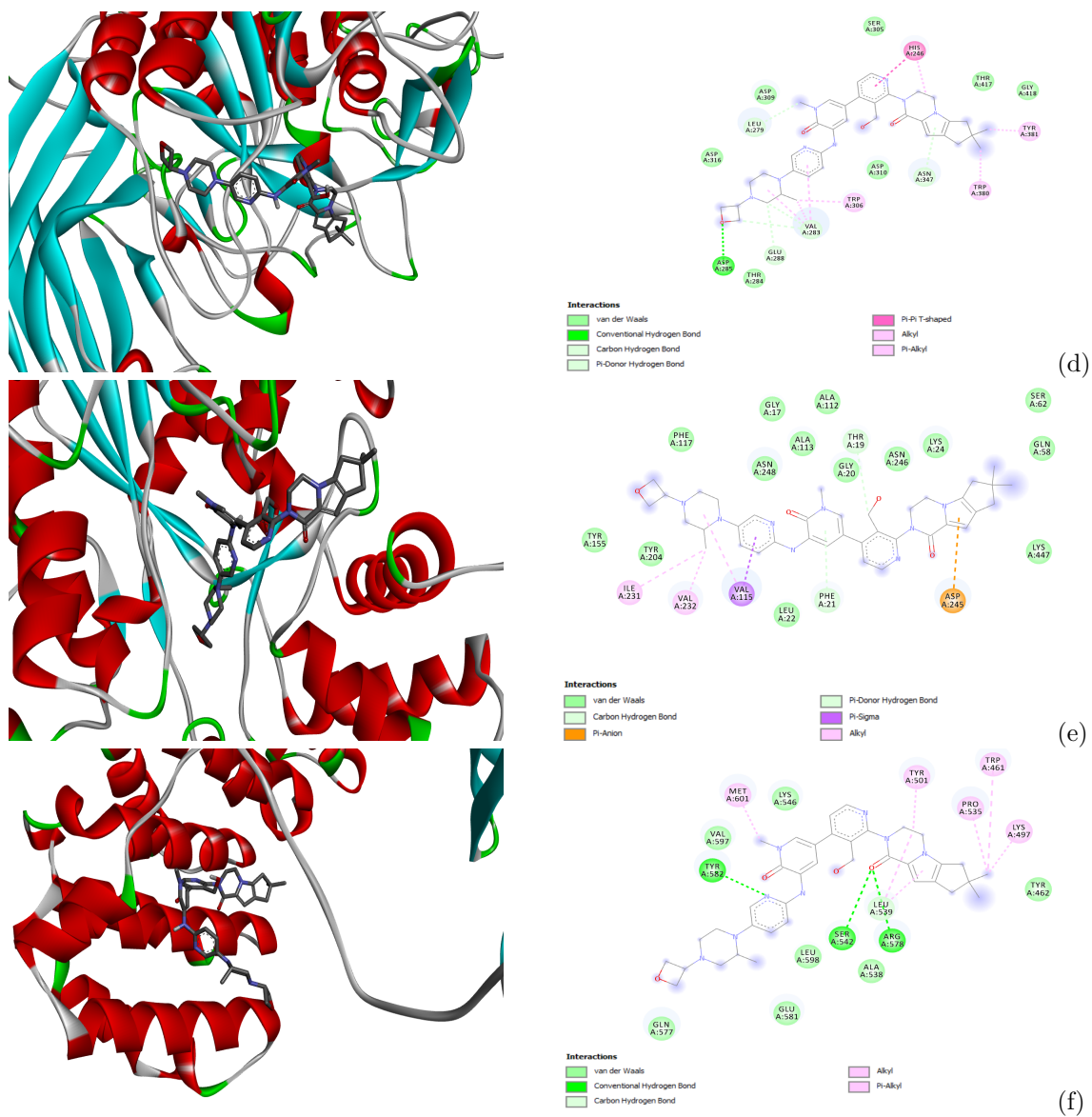


Figure S9: The binding conformations and 2D-interactions of Fenebrutinib on the targeted proteins predicted by using Autodock: (d) Fenebrutinib on Proprotein convertase subtilisin/kexin type 6. (e) Fenebrutinib on Fatty acyl-CoA reductase 2. (f) Fenebrutinib on AP-2 complex subunit alpha-2.

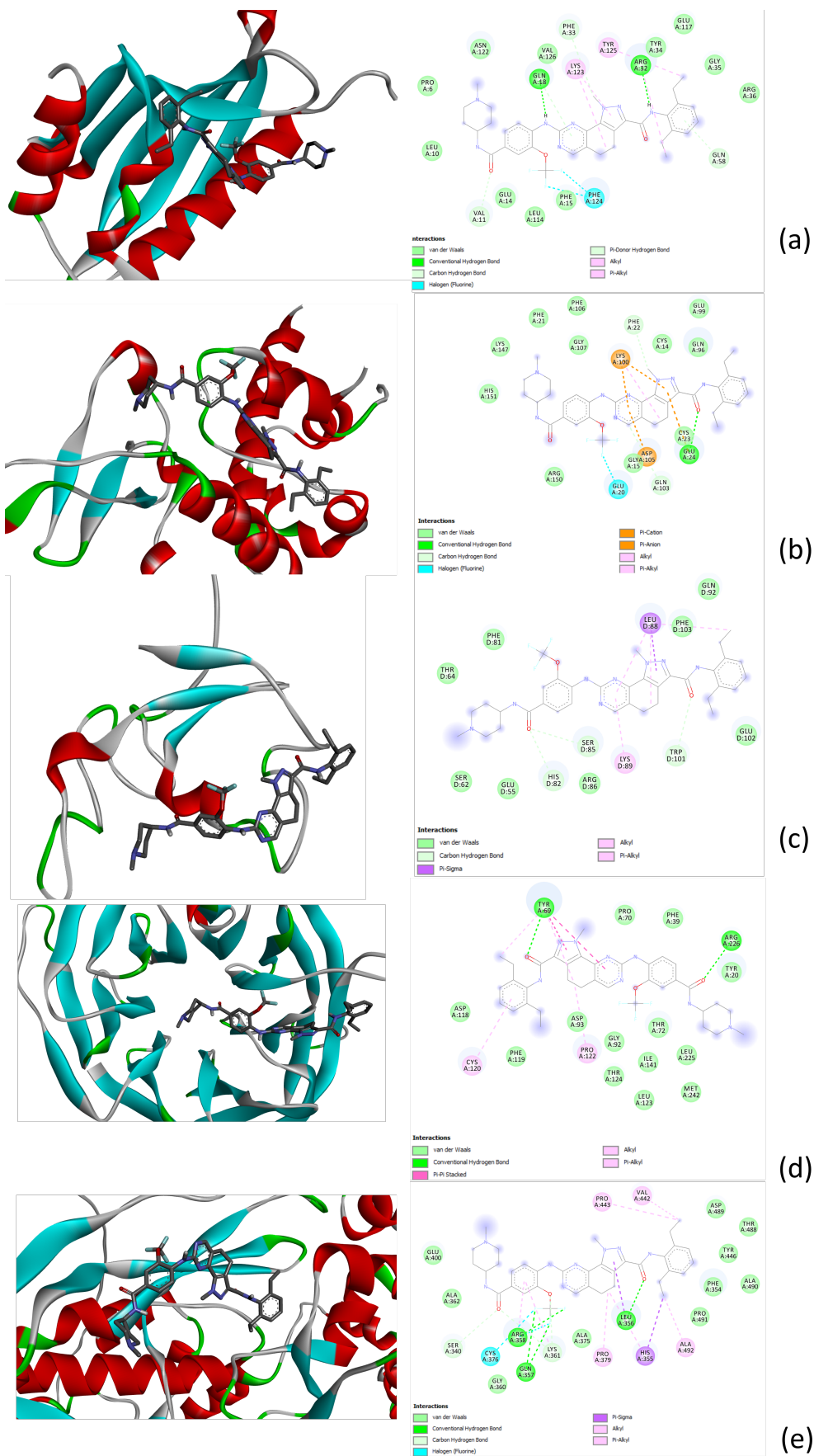


Figure S10: The binding conformations and 2D-interactions of NMS-P715 on the targeted proteins predicted by using Autodock: (a) NMS-P715 on Ras GTPase-activating protein-binding protein 2. (b) NMS-P715 on Casein kinase II subunit beta. (c) NMS-P715 on E3 ubiquitin-protein ligase RBX1. (d) NMS-P715 on DDB1- and CUL4-associated factor 7. (e) NMS-P715 on tRNA (guanine(26)-N(2))-dimethyltransferase.

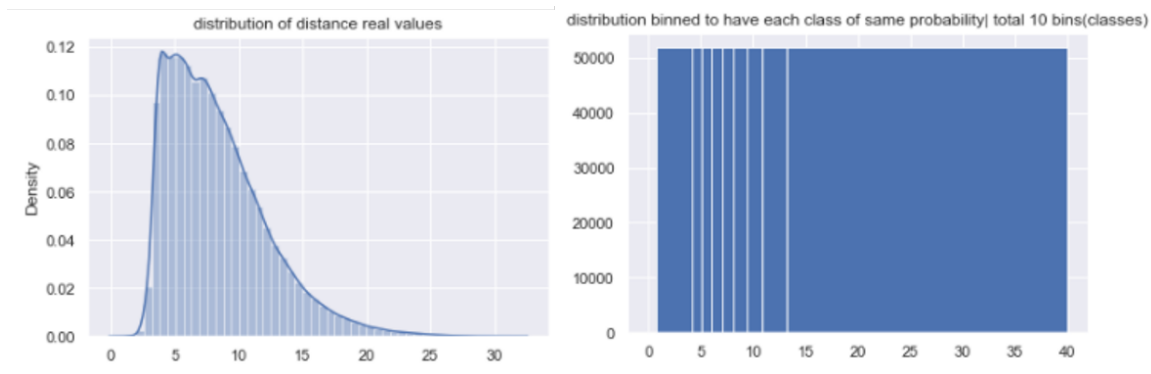


Figure S11: Histogram equalization results: the left panel shows the original distribution of distance real values; to formalize a multi-class classification where each class has equal probability, histogram equalization transforms the distribution to the right panel of 10 bins, each as a class.

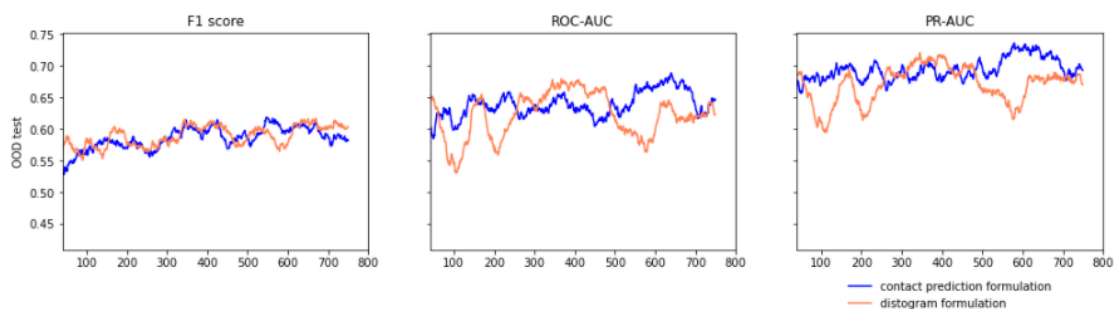


Figure S12: Ablation study to compare the impact of two formulation of protein structure distance prediction, contact prediction v.s. distogram prediction. The two variants have similar OOD-test performance.

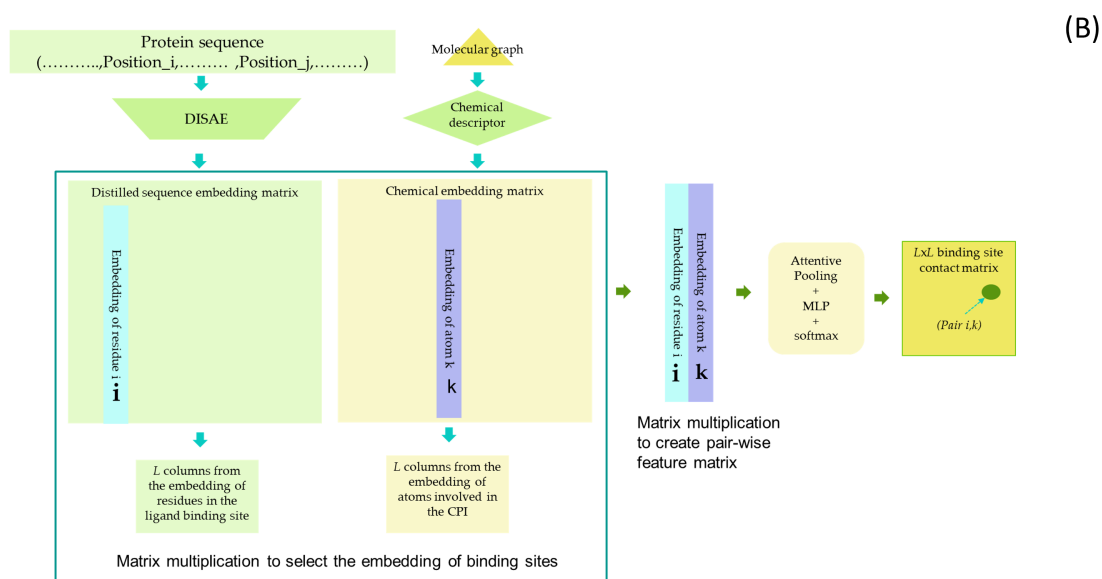
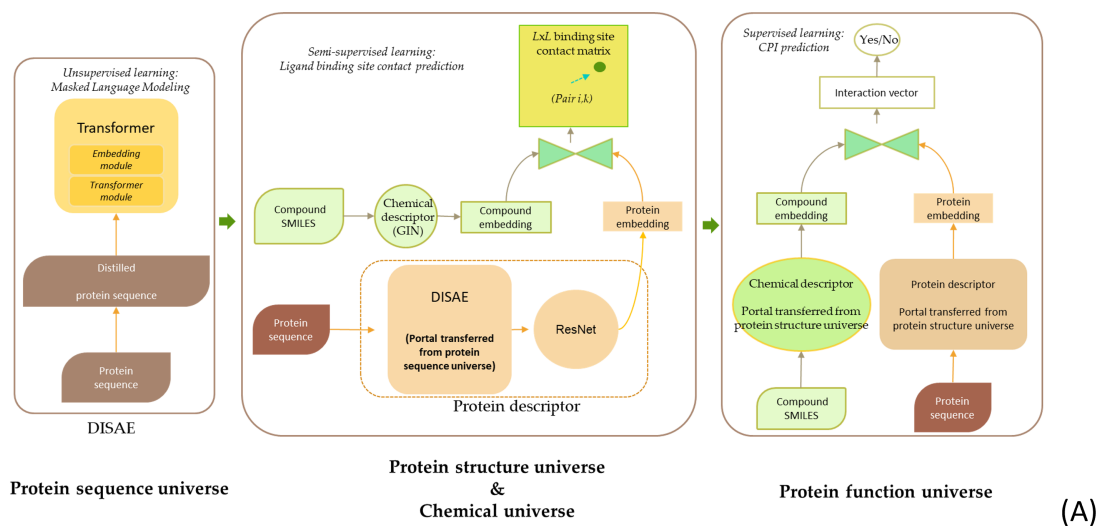


Figure S13: Illustration of PortalCG architecture: (A) the pipeline of STL (B) The model architecture for predicting binding site distance matrix. Note that Portal Learning is a general framework at the training scheme level instead of at the model architecture level. OOC-ML as an optimization algorithm is only used in the protein function universe which is not a model architecture component (See Figure 1).